Title: WIF1 re-expression in glioblastoma inhibits migration through attenuation of non-canonical WNT signaling by downregulating the lncRNA MALAT1.
Authors: Vassallo I, Zinn P, Lai M, Rajakannu P, Hamou MF, Hegi ME
Journal: Oncogene
Year: 2016 Jan 7
Volume: 35
Issue: 1
Pages: 12-21
DOI: 10.1038/onc.2015.61

Vassallo et al. Oncogene *35*, 12-21, 2016. PMID: 25772239

WIF1 re-expression in glioblastoma inhibits migration through attenuation of non-canonical WNT signalling by downregulating the lncRNA MALAT1.

Irene Vassallo,[1,2] Pascal Zinn,[3] Marta Lai,[4] Premnath Rajakannu,[1,2] Marie-France Hamou,[1,2] Monika E. Hegi[1,2]

[1]Neurosurgery (NCH) and [2]Neuroscience Research Center (CRN), Lausanne University Hospital (CHUV), Lausanne, Switzerland; [3]Neurological Surgery, Baylor College of Medicine, Houston, TX, USA; [4]Laboratory of Functional and Metabolic Imaging (LIFMET), Ecole Polytechnique Fédérale de Lausanne, Lausanne, Switzerland

Abstract

Glioblastoma is the most aggressive primary brain tumor in adults and due to the invasive nature cannot be completely removed. The WNT inhibitory factor 1 (WIF1), a secreted inhibitor of WNTs, is systematically downregulated in glioblastoma and acts as strong tumor suppressor. The aim of this study was the dissection of WIF1 associated tumor suppressing effects mediated by canonical and non-canonical WNT-signalling. We found that WIF1 besides inhibiting the canonical WNT pathway selectively downregulates the WNT/Calcium pathway associated with significant reduction of p38-MAPK phosphorylation. Knock-down of WNT5A, the only WNT ligand overexpressed in glioblastoma, pheno-copied this inhibitory effect. WIF1 expression inhibited cell migration in vitro and in an orthotopic brain tumor model, in accordance with the known regulatory function of the WNT/Ca2+ pathway on migration and invasion. In search of a mediator for this function differential gene expression profiles of WIF1-expressing cells were performed. MALAT1, a long non-coding RNA and key positive regulator of invasion, emerged as the top downregulated gene. Indeed, knock-down of MALAT1 reduced migration in glioblastoma cells, without effect on proliferation. Hence, loss of WIF1 enhances the migratory potential of glioblastoma through WNT5A that activates the WNT/Ca2+ pathway and MALAT1. These data suggest the involvement of canonical and non-canonical WNT-pathways in glioblastoma promoting key features associated with this deadly disease, proliferation on one hand and invasion on the other. Successful targeting will require a dual strategy affecting both canonical and non-canonical WNT pathways.

Introduction

Glioblastoma (GBM) is the most frequent and most malignant primary brain tumor in adults. Despite a multidisciplinary therapeutically approach comprising maximal safe surgical resection, followed by radiotherapy (RT) with concomitant and adjuvant temozolomide, the prognosis is extremely dismal, with a median overall survival of 15 months.[1] Due to the infiltrative nature GBM almost invariably recur[2] hence, therapeutic advances for GBM will require a better understanding of the primary mediators of the invasive behaviour with the aim to identify druggable targets.

WNT signalling is involved in diverse processes, from early embryonic patterning to regulation of stem cell self-renewal and differentiation.[3-5] WNT pathway dysregulation can dramatically alter differentiation and cell fate decisions,[6] thus it is not surprising that abnormalities in WNT signalling are found in a wide range of cancers. The most prominent is colorectal cancer where β-catenin-dependent signalling, also known as canonical WNT signalling plays a crucial role. Aberrant activation of the pathway is mainly mediated by destructive mutations in adenomatous polyposis coli (APC, 80%), prohibiting destruction of β-catenin, or activating mutations in β-catenin (5%).[7, 8] In contrast, the non-canonical WNT pathways, for which WNT5A is a prominent ligand, has been reported to exert a tumor suppressive effect on colon cancer.[9] The role of activated WNT pathways in GBM is not as clear. The pathway is not targeted by mutations in APC or β-catenin, however, several negative regulators have been shown to be inactivated, mainly by epigenetic silencing and/or deletion, and few mutations.[10-12] Furthermore, aberrant signalling of both the canonical and the non-canonical signalling pathways seem to contribute to the

aggressiveness of GBM. Aberrant β-catenin activation has been associated with maintenance of glioma-initiating cells (GICs),[13] while non-canonical WNT signalling with increased invasion.[14, 15] We previously described WNT inhibitory factor 1 (*WIF1*) gene as a strong tumors suppressor gene in GBM where it is targeted by deletion and/or promoter methylation.[10] WIF1 is a secreted WNT inhibitor that works by sequestering soluble WNT proteins. It prevents the interaction between WNT morphogens and their specific receptors and it has been shown to bind to virtually all WNT agonists.[16] In contrast to other WNT inhibitors like dickkopf (DKK) family members that can inhibit only the β-catenin dependent pathway, WIF1 can block the activation of both canonical and non-canonical WNT signalling pathways. Here we focused on the analysis of two main non-canonical WNT pathways, namely WNT/JNK and WNT/Ca^{2+} to tie down the relationship between WIF1 expression and WNT signalling alterations.

Results

WIF1 expression inhibits both the β-catenin- and the WNT/Ca^{2+} pathways without affecting WNT/JNK signalling.

To identify the molecular pathways involved in the tumour suppressive-phenotype we set out to analyse both the canonical and several of the known non-canonical WNT signalling pathways. To this effect, a WIF1-inducible GBM cell line LN-229_ind*WIF1* (TET-ON system) was constructed that co-expresses dsRed as marker. The WIF1-mediated tumour-suppressing activity was confirmed in this model after orthotopic injection of the cells into the mouse brain. Mice treated with DOX had a significantly longer survival (p-value of log-rank test = 0.0062) (Supplementary Figure 1). The transactivation analysis of the β-catenin (TRF) promoter confirmed a modest, WIF1-mediated downregulation of the canonical-WNT pathway using a luciferase based-reporter system (Figure 1A). Then we focused on WIF1 function in non-canonical WNT-pathways. Expression of WIF1 had no impact on transactivation of the AP1 promoter, although the reporter was sensitive to activation by phorbol-12-myristate-13-acetate (PMA, 6h, 200nM). The AP1 reporter serves as readout for WNT/JNK pathway activation,[17-19] a non-canonical WNT signalling pathway involved in the regulation of the cytoskeleton and cell adhesion.[20] No effects were observed in the control cell line LN-229_ind_dsRED that upon DOX treatment only induces dsRED (Supplementary Figure 2A-B). Next we investigated the non-canonical WNT/Ca^{2+} pathway, a signal transduction pathway involved in regulation of cellular migration and invasion.[21] The activation was tested using a fluorogenic Ca^{2+} binding assay, in which induced fluorescence is proportional to the Ca^{2+}

concentration ([Ca^{2+}]) in the cytoplasm. Since the DOX induced LN-229_ind*WIF1* cells also express dsRED, which interferes with the fluorochrome in this assay, the [Ca^{2+}] was measured in LN-229 cells transfected with either a *WIF1* expression vector or the respective empty vector. *WIF1* expression consistently reduced the [Ca^{2+}], suggesting involvement in WNT/Ca^{2+} signalling (Figure 1B).

WIF1 significantly reduces the phosphorylation of both p38-MAPK and ERK

We then analysed the phosphorylation profile of 46 kinases to determine which signalling pathways were modulated by WIF1 induction. A significant reduction was detected in the phosphorylation of both p38-MAPK (ratio ind_WIF1/control of 0.48) and ERK (ratio ind_WIF1/control of 0.75) (Figure 2 A-B). Minor inhibition of phosphorylation was also detected for phospho-CREB, phosho-MSK1/2 and phospho-p70, which all are downstream of ERK and p38-MAPK. In contrast, no changes in phosphorylation of either JNK protein or c-Jun were observed, in accordance with the findings of the AP1 pathway analysis. Western blot analysis of LN-229 transfected with either *WIF1* or the empty vector confirmed the reduction of phospho-ERK and phospho-p38-MAPK. However, no changes in phosphorylation were detected for the mitogen-activated protein kinase (MAPK) kinase 3 (MKK3), a known regulator of p38-MAPK (Figure 2C-D and Supplementary Figure 3A). To analyze the effect of p38-MAPK and ERK1/2 inhibition on intracellular calcium and to test whether the two pathways are causally linked we inhibited them separately with specific small molecules inhibitors. Inhibition of p38-MAPK reduced phosphorylation of MAPKAPK-2, a direct p38-MAPK target (Supplementary Figure 4A,B) and significantly diminished the [Ca^{2+}](Figure 2E), while no effect was observed on

ERK phosphorylation (Supplementary Figure 4C). ERK inhibition achieved with the specific MEK1/2 inhibitor U0126, neither affected the [Ca^{2+}] (Figure 2E), nor p38-MAPK phosphorylation (Supplementary Figure 4D). Taken together this suggests that there is no direct cross-talk between p-38MAPK and ERK 1/2.

WNT5A **depletion recapitulates the alterations induced by** ***WIF1*** **expression.**

WNT5A has been described as a regulator of the non-canonical WNT pathway that controls p38-MAPK activity and [Ca^{2+}].[22] Despite WNT ligands being expressed in GBM, only *WNT5A* is overexpressed in GBM relative to non-tumoral brain as determined by analysing two GBM gene expression datasets. The fold change for *WNT5A* was 3.1 in our dataset,[23] and 2.5 in the GBM-TCGA_Agilent set[24] (Figure 3A). This begged the question whether downregulation of WNT5A would phenocopy both, the inhibition of p38-MAPK and the reduction of the [Ca^{2+}] observed with WIF1 re-expression. Downregulation of *WNT5A* using two specific siRNAs (Supplementary Figure 5A-B), reduced the phosphorylation levels of both p38-MAPK and ERK (Figure 3B-C, Supplementary Figure 3B) and the intracellular [Ca^{2+}] (Figure 3D), recapitulating the phenotype induced by WIF1 expression.

WIF1 expression reduces tumor cell migration ***in vitro*** **and** ***in vivo***

Since the WNT/Ca^{2+} signalling is essential for regulation of migration we tested whether WIF1 expression influenced the invasive potential of GBM cells. WIF1 expression significantly reduced migration in both, the trans-well assay and the wound-healing assay (Figure 4A,B). Proliferation of LN-229_ind*WIF1*

was analyzed to verify that reduction in migration was not a consequence of differences in cell growth. Indeed, WIF1 mediated inhibition of growth was only detectable after 4 days of culture, thus supporting an inhibitory effect on migration (Figure 4C). Furthermore, neither migration nor proliferation were affected in the control cell line (LN-229_ind_*dsRED*) in which DOX exposure induces only *dsRED* expression (Supplementary Figure 2C, D). Next we aimed at investigating the relevance of the biological effect of WIF1 observed *in vitro* in the GBM derived sphere-line LN-2669GS, a more relevant GBM model. GBM sphere lines maintained under stem cell conditions retain some tumor stem cell properties and most importantly, the ability to grow invasively when xenografted orthotopically into the brain of mice, hence recapitulating this important original feature of GBM. Ectopic expression of *WIF1* in LN-2669GS (LN-2669GS_*WIF1*) reduced the sphere-forming potential *in vitro* as compared to the respective empty vector control (LN-2669GS_IRES) (Figure 5A). Next the sphere lines were injected orthotopically into the brain of nude mice to evaluate tumorigenicity and invasiveness modulated by WIF1. Mice were sacrificed at the appearance of the first neurological symptoms, such as ataxia and lethargy, or body weight loss, clear signs of tumor growth. The brains were collected, formalin fixed and cut in coronal slices. The Kaplan–Meier curves confirmed the tumor suppressing function of WIF1 expression in the GBM sphere line LN-2669GS (log-rank test, p= 0.0046 (Figure 5B). The sections taken in the plane of the injection were immunostained for the human specific antibody anti–Nucleolin to identify the human tumor cells. Migration was measured by comparing the number of human tumor cells on the injected versus the contra-lateral side, in the plane of the injection (Figure 5C). At the time of sacrifice,

which means the mice were moribund due to the tumor burden, the *WIF1* transduced cells (LN-2669GS_*WIF1*) had migrated less to the contra-lateral side, reflected in a statistically smaller ratio than the control cells (LN-2669GS_IRES) (Figure 5D, E). Hence, suggesting a WIF1-dependent reduced migratory capacity *in vivo*.

WIF1 regulates the expression of _MALAT1_, a key positive regulator of migration.

In order to identify new genes regulated by WIF expression, differential gene expression profiles were obtained for LN229_ind*WIF1* 48h after induction. The time point for the analysis was motivated by the kinetics of *WIF1* induction and secretion of WIF1 into the medium. At 48h the WIF1 concentration in the medium reached a plateau (Figure 6A). Figure 6B shows the heat map of the most variable transcripts presented as logarithmic fold change compared to the non-induced samples (duplicates). We selected the probes with a log fold change of > |1|. Several interesting candidate transcripts emerged, which were then tested in additional experiments by qRT-PCR in LN-229_ind*WIF1* (Figure 6C), and in the GBM cell line LN-319 and the sphere line LN-2669GS transduced with *WIF1* (Supplementary Figure 4A-C). Across the three lines the most consistent *WIF1*-dependent change was downregulation of the metastasis associated lung adenocarcinoma transcript 1 (*MALAT1*), which was subsequently chosen for further investigations. *MALAT1* is a nuclear long non-coding RNA, whose expression has been associated with a migratory phenotype in several cancer types[25-28] however nothing has been reported from GBM. *MALAT1* was found overexpressed in GBM as compared to non-tumoral brain (fold change= 1.4, p-

value= 0.0062) in our data set.[23] Next we wanted to elucidate the mechanism for WIF1 mediated downregulation of *MALAT1.* Both *WNT5A* depletion (Figure 6D) and p38-MAPK inhibition (Figure 6E) lead to a drastic reduction in *MALAT1* transcription. Since *WNT5A* depletion, in contrast to *WIF1* induction, does not affect the canonical WNT pathway, as measured by *AXIN2* expression, we conclude that *MALAT1* expression is dependent on activation of the non-canonical WNT pathway.

MALAT1 downregulation inhibits invasion without affecting growth

MALAT1 was depleted by two siRNAs to test the involvement of *MALAT1* in migration of LN-229. The efficacy of the RNAi procedure was assessed by qRT-PCR, measuring expression of *MALAT1* at two different time points, 48 and 72h. To provide functional evidence for downregulation of *MALAT1* the expression of two known target genes of *MALAT1* were determined, collagen triple helix repeat containing 1 (*CTHRC1)* and solute carrier family 26 (anion exchanger), member 2 (*SLC26a2).*[26] Both *MALAT1* and the respective target genes displayed significant downregulation (Figure 7A). The migratory potential of LN-229 depleted of *MALAT1* was tested using both the wound healing assay and the transwell assay. The wound-healing assay was performed starting 48h after the siRNA transfection. Downregulation of *MALAT1* was sufficient to significantly reduce the area of the scratch covered (Figure 7B, C). Similarly, the transwell assay confirmed a reduction in migration of *siMALAT1*-transfected cells (Figure 7D, E). Importantly, growth was not affected by downregulation of *MALAT1*, thus the results obtained were indeed related to a deficit in migration rather than a difference in growth rate (Figure 7F). The inhibitory effect of *MALAT1* on

migration was recapitulated in two additional GBM cell lines (LN-18 and LN-428, Supplementary Figure 7).

Discussion

Little is known about the role of the WNT pathways in the malignant behaviour of human GBM. We previously provided evidence for the tumor suppressing function of WIF1 in GBM.[10] Here we addressed the question of WIF1 mediated mechanisms implicated in both the canonical and non-canonical WNT pathways. *WIF1* expression inhibited the canonical as well as the WNT/Ca^{2+} signalling pathway in GBM cells. The WIF1 mediated decrease in intracellular [Ca^{2+}] was found to be associated with a significant inhibition of p38-MAPK phosphorylation, in line with findings in mouse F9 teratocarcinoma cells.[22] However, no effects were detected either on AP1-based reporter activity or phosphorylation of JNK and c-Jun, although JNK-AP1 signalling has been suggested to contribute to the malignant phenotype in GBM.[14, 29] *WNT5A* depletion was sufficient to recapitulate the effect observed for WIF1 expression, with downregulation of phospho-p38-MAPK and reduction of the intracellular [Ca^{2+}]. Hence we are providing first evidence, for an important role of WNT5A/p38-MAPK/Ca^{2+} mediated non-canonical WNT signalling in GBM. Both *WNT5A* expression and p38-MAPK activation can have opposite effects depending on the cellular context. WNT5A-dependent non-canonical signalling has been described to be tumor-suppressive in several types of cancer such as ovarian and colorectal cancer.[30-33] However, in GBM, WNT5A has been associated with tumor aggressiveness, as its expression has been reported to be essential for the maintenance of the invasive phenotype.[14, 15, 34] Moreover it has been

reported that stable depletion of WNT5A in a GBM cell line induced senescence,[35] which is in line with our previous report showing increased senescence in GBM cell lines ectopically expressing *WIF1*.[10] The importance of WNT5A in GBM is also supported by the fact that it is the only WNT ligand whose expression is overexpressed as compared to non-tumoral brain.

Similar considerations are also valid for p38-MAPK activation. Although p38-MAPK is involved in the regulation of a plethora of responses, including pro-apoptotic pathways,[36] the final effect is cell-type specific and, in GBM, there is evidence that p38-MAPK activation correlates with malignancy and with the invasive potential.[37-39]

Both the WNT/Ca^{2+} pathway and activation of p38-MAPK are involved in the regulation of cell migration in normal development as well as in cancer progression.[40, 41] Here we provided evidence that in addition to loss of tumorigenicity;[10] *WIF1* expressing cells reduce migration both *in vitro* and *in vivo*. Moreover, we discovered that the most downregulated gene upon *WIF1* induction was *MALAT1,* a non-coding RNA known to be a *s*trong positive regulator of invasion. Physiologically, *MALAT1* localizes to nuclear speckles and regulates alternative splicing by modulating the distribution and levels of splicing factors.[27, 42] *MALAT1* has been associated with cell migration and invasive properties of cancer.[26, 28] In GBM, *MALAT1* has not yet been investigated. Here we have clearly shown that *MALAT1* expression is regulated by *WIF1* expression via the WNT5A/p38-MAPK/Ca^{2+}-non-canonical WNT signalling axis. Moreover, *MALAT1* expression proved to be extremely important for the maintenance of the migratory potential of GBM cell lines.

Virtually all GBMs recur which is attributed to the extremely high capability of GBM cells to migrate and to invade the surrounding normal brain structures, precluding complete surgical resection, and effective targeting by irradiation.[43] A better understanding of the key regulatory pathways contributing to the migratory potential of GBM is required for development of successful therapeutic strategies. *MALAT1 per se*, would probably not be a good candidate because of its high basal level of expression in normal brain. Furthermore, *MALAT1* is involved in regulation of numerous genes. Hence, identification of the most important effectors of *MALAT1* related to invasiveness would be the next logical step.

Taken together, our results clearly show that the final tumor suppressive phenotype induced by *WIF1* is a combination of the inhibition of both canonical and non-canonical WNT pathway(s) as depicted in the model from Figure 8. We hypothesize that inhibition of the canonical pathway mediates decreased growth, while inhibition of the non-canonical WNT pathway leads to decreased migration. We suggest that inhibition of the non-canonical WNT pathway by WIF1 is mediated by sequestration of WNT5A that results in decrease of p38-MAPK phosphorylation, drop of intracellular $[Ca^{2+}]$, and reduction of *MALAT1* expression, resulting in attenuated migration. These findings should be taken into account when developing WNT inhibitors for therapy, as the canonical WNT pathway should not be targeted alone, but rather in combination with inhibition of non-canonical WNT pathway(s) in order to both inhibit tumor growth and migratory properties.

Material and Methods

Cell lines

The adherent GBM cell lines LN-229, LN-319, LN-18 and LN-428, have been established in our lab as well as the sphere line LN-2669GS.[44, 45] The lines were authenticated by DNA fingerprinting.[46] The adherent cell lines were cultured in Dulbecco's modified Eagle's medium (DMEM, Invitrogen), supplemented with 5% fetal calf serum (Hyclone) and 100 units/ml penicillin & streptomycin (Invitrogen). The sphere line LN-2669GS was cultured under stem-cell conditions using DMEM/F12 medium containing B27 supplement and 20 ng/ml of both epidermal growth factor (EGF) and fibroblast growth factor 2 (FGF2). LN-229_ind*WIF1* and LN-229_ind_dsRED were treated with doxocyclin (DOX, Clontech) at 1µg/ml. The following small molecule inhibitors were used: SB203580 (Calbiochem, La Jolla, CA) and SB239063 (SIGMA, cat# S0569) specific for p38-MAPK, and the MEK 1/2 inhibitor U0126 (Cell Signalling # 9903) for the inhibition of ERK 1/2.

Gene Expression Datasets

Gene expression profiles from our GBM cohort was previously described Murat et al. (HG133 Plus 2.0, GBM=70, Non Tumoral brain=4, excluding 10 recurrent GBMs)[23] and is deposited in the Gene Expression Omnibus (GEO) database at http://www.ncbi.nlm.nih.gov/geo/ (accession-number GSE7696). The molecular profiles of GBM from The Cancer Genome Atlas (TCGA) project were downloaded (Level 3 data, Agilent 244K Custom Gene Expression G4502A-07, GBM=573, Non Tumoral brain=10) (http://tcga-data.nci.nih.gov/tcga/tcgaHome2.jsp[24, 47]

Plasmids and Small Interference RNAs

The WNT-β-catenin activity luciferase reporter vectors TOP_FLASH and FOP_FLASH and the fusion construct expressing LEF1-β-catenin were generous gifts of Prof. Tatiana Petrova.[48] The reporter for AP1 signalling, pGL3-5xTRE-TATA was used to measure the AP1 signalling pathway. The pRL CMV Renilla luciferase (Promega AG) plasmid was used to normalize for transfection efficiency. The two *WIF1* expression vectors (pcDNA3.1_*WIF1* and pIRES2_EGFP_*WIF1*) were described in Lambiv et al.[10] The list of siRNAs is available in Supplementary Table 1.

Cell transfection and generation of stable cell lines

Transfections were performed using the NEON electroporator (Invitrogen). For adherent cell lines the parameters were set at 1400 V, 20 ms pulse width, 1 pulse, while for sphere cell lines the voltage was increased to 1700 V. The ratio of DNA/cells was usually 20µg of DNA/4*10^6 cells, while the final concentration of transfected siRNA was 25 nM for si*WNT5A_#1* and #2 and 15 nM for si*MALAT1*_#1 and 25nM for si*MALAT1*_#2.

For stable transfections, cells were transfected with the expression vector followed by selection with G418 (G418, Geneticin®, Gibco). Resistant clones were selected and maintained in 400-800 µg/ml of G418. The inducible cell line LN229_ind*WIF1* was constructed transfecting the following three vectors: the reverse tetracycline transactivator (rtTA), plasmid pUHG 17.1 [49] and plasmid pJ6Ω,[50] containing the puromycin resistance gene (Puromycin Dihydrochloride, Calbiochem No. 540222, (1µg/ml)), and either the pTRE-Tight-BI-DsRed-Express vector (Clontech Catalog No. 631065) into which the *WIF1* cDNA was cloned, or

the respective empty vector for the control cell line (LN229_ind_*dsRED)*. The vector contains an inducible bidirectional promoter that beside the gene of interest expresses the red fluorescent protein (dsRED_Express).

Luciferase-based assays:

Lusiferase experiments were performed using the DUAL Luciferase system (Promega) as suggested by the manufacturer. Luminescence was measured two days after transfection with the respective plasmid and analyzed using a Synergy H1 Hybrid Multi-Mode Microplate Reader.

Intracellular calcium measurement:

Intracellular [Ca^{2+}] was determined using the Fluo-Forte® Calcium Assay Kits (Enzo Life Sciences, USA) as suggested by the manufacturer 48h after transfection. Fluorescence was measured using a Synergy H1 Hybrid Multi-Mode Microplate reader (ex. 485 and em. 520 nm).

Proliferation assay:

Growth curves were established as described previously,[10] briefly 2×10^4 cells were seeded in 12 well plates. At every time point, cells were washed with PBS, and stained with 500 µl of crystal violet solution. Plates were left to dry, and 500 µl of 1% sodium dodecyl sulfate (SDS) in distilled water was added per well. Absorbance was then measured at 595 nm. Growth in soft agar was determined in 6-well plates containing 2 ml of 1% agar in complete medium as the bottom layer, and 1 ml of 0.4% agar in complete medium as the top layer. Two × 10^3 cells were seeded in triplicate. After 3 weeks the number of colonies was determined

with an inverted phase-contrast microscope. Cluster of 50 cells was scored as colony. For the sphere formation assay using limiting dilution the cells were dissociated into single-cell suspensions, and then plated into 96-well plates with various seeding densities (from 250 to 750 cells per well). Two to 3 weeks later each well was examined for the formation of spheres.

Cell migration assays

Transwell (Corning), with 8.0 µm pores were used to measure migration. $1x10^4$ cells were suspended in 100 µl of DMEM containing 0.5% FCS and transferred to the upper chamber and 600 µl of 5% FCS medium were applied to the lower chamber. After 16-18h, the cells on the upper side of the filters were wiped off and the cells that migrated to the lower side were stained with crystal violet. To perform the scratch assay, the cells were plated onto 35-mm-diameter dishes and the monolayer of cells was manually scratched with a plastic tip. After being washed with PBS, pictures were taken to set the time (T) zero. Pictures were taken at the identical spot at 24h and 48h. The area of the scratch not yet covered by cells was quantified using ImageJ software,[51] and the data are shown as % of covered scratch (T zero = 0%). For the experiment performed with the LN-229_ind*WIF1*, the cells were seeded 24h before induction with DOX, and the scratch was performed 24h after DOX treatment. For the transwell assay cells were seeded in the upper chamber 48h after induction.

Intracranial Nude Mouse Tumorigenicity Assay

The protocol was authorized by the local veterinary authorities (VD1181.3-6). Six-weeks-old Swiss nu/nu mice were stereotactically injected with $1X10^5$ cells,

resuspended in 5 µl (coordinates from the bregma: 0.5 mm anterior, 2 mm lateral, 3 mm depth, stereotactic frame, Stoelting). Mice were sacrificed at first appearance of neurological symptoms (lethargy, ataxia, and seizures) or body weight loss. To test intracranial tumorigenicity of LN-229_ind*WIF1* mice were fed with DOX supplemented food (625 µg/kg, Harlan TD.01306 Rodent Diet, changed every 2-3 days), the controls received standard food.[52] For survival analyses, 10 mice were used per group for the LN-2669GS while 6 mice per group for the LN-229_ind*WIF1*.

Protein analysis

Proteins were extracted from dry pellets of frozen cells (–80 °C) as described previously.[10] Briefly, the pellets were dissolved in RIPA buffer, supplemented with protease-inhibitor (Complete Mini, Roche) and Phosphatase-inhibitor (PhosSTOP, Roche). The lysate was centrifuged at 14,000 g for 10 min at 4°C. The supernatant was collected as whole cell lysate. Protein concentration was measured using the Bradford assay (Bio-Rad Laboratories). The protein samples were subjected to reducing SDS-PAGE using standard methods, using 40 µg for total-protein and 90 µg for phospho-protein analysis. Western blots were probed with the following antibodies (Cell Signalling) at a dilution 1:1000: phospho-MKK3/6 (#9231), phospho-p38-MAPK (#9211), p38-MAPK (#9212), Phospho-p44/42 MAPK -Erk1/2 (#9106), p44/42 MAPK -Erk1/2 (#9102), Phopsho-MAPKAPK-2 (#3007), MAPKAPK-2 (#3042). The expression of α-Tubulin (Sigma, T-6074, 1:3000) served as loading control. The Human Phospho-Kinase Antibody Array (R&D system, ARY003) was used according to the manufacturer's instructions using 300 µg of protein.

Enzyme-Linked Immunosorbent Assay

The cell supernatant, collected and it was quantified for secreted WIF1 with a sandwich enzyme-linked immunosorbent assay (R&D System) following the manufacturer's instructions. Data were normalized to the cell number.

Immunohistochemistry and quantification of migration *in vivo*

At sacrifice mouse brains were extracted and either snap frozen or formalin fixed for 4h, cut into coronal slices, and paraffin embedded (FFPE) for further analyses. Sections were stained with Hematoxylin and eosin, and glial fibrillary acidic protein (GFAP) using standard procedures. For the identification of human (tumor) cells, sections were stained for human Nucleolin using the protocol kindly provided by Donna Senger. Slides were treated in citrate buffer pH6 at 95°C for 60 min, followed by 121°C for 8 min (under pressure) to retrieve the antigen. Sections were treated sequentially with H2O2 (1%, 10 min), avidin and biotin blocking solution (SP-2001) according to the manufacturer's instructions, and rodent block M treatment (15 min, RBM961, BIOCARE MEDICAL). The primary antibody anti-human Nucleolin (cat No. 13541, Abcam) was applied at a dilution of 1:200 (1 h), followed by the secondary antibody, horse anti-mouse using the Avidin-Biotin kit (BA-2001, VECTOR), revelation was allowed for 2 to 4 min according to manufacturor's instructions (ImmPACT DAB reagent, SK-4105, VECTOR). The washing steps were performed with TBS-0.05% Tween20. Stained sections were scanned and tumor cells were quantified by counting the Nucleolin positive cells over a surface of 500 μm^2. This procedure was performed both on the area close to the injection site and on the contra-lateral side to generate a

ratio of number of tumor cells in the contra-lateral side/number of tumor cells in the injected side. The ratio is reported as quantification tumor cell migration *in vivo*.

RNA Isolation and Reverse Transcription PCR

Total RNA was extracted using the RNeasy total RNA extraction kit (Qiagen), and cDNA was synthesized using PrimeScript RT-PCR Kit (TAKARA). Real-time quantitative PCR was performed with Fast Sybr Green Master Mix (Applied Biosystem) using the Rotor Gene 6000 Real-Time PCR system (Corbett Life Science). The quality of the products was controlled by the melting curve. Transcript levels were normalized against human *GAPDH.* [53] Already published primers were used for the following genes: *WIF1*[10]; *AXIN2*[54]); *WNT5A*[55], *IL6*[56]. Primers were designed using Primer3 [57] (Supplementary Table 2).

***WIF1*-induced LN-229 gene expression profile**

The LN-229_ind*WIF1* were seeded (3x10^5 cells/small flask, area 2500 mm^2) and let adhere for 24h and then half of the flasks were induced with DOX. Cells were harvested 48h after induction, and RNA was extracted. The samples expression profiles were generated on the Affymetrix GeneChip HG-U133 Plus 2.0 microarray platform (Affymetrix, Santa Clara, CA) at the Genomics Platform at the University of Geneva. The analyses were carried out in R (http://www.R-project.org/), using Bioconductor packages.[58] Raw CEL files were processed using the robust multichip average (RMA) algorithm available in the Affy package.[59] Probes were filtered using the coefficient of variation.

Statistical analysis

The Student t test was used to compare continuous variables between two groups. Survival is visualized by Kaplan-Meier curve and analyzed using the log-rank test. P values less than 0.05 were considered statistically significant. Results are marked with 1 asterisk (*) if $p< 0.05$ and 2 (**) if $p < 0.01$ and with 3(***) if $p<0.001$. All statistical tests were two-sided. Data are presented as mean values with standard deviation.

Conflict of interest

The authors declare no conflict of interest.

Acknowledgments

The presented work was supported by the Swiss National Science Foundation (31003A_138116 / 1). The results published here are in part based upon data generated by The Cancer TCGA Genome Atlas pilot project established by the NCI and NHGRI. Information about TCGA and the investigators and institutions who constitute the TCGA research network can be found at http://cancergenome.nih.gov/.

Supplementary Information accompanies the paper on the Oncogene website (http://www.nature.com/onc)

References:

1 Stupp R, Mason WP, van den Bent MJ, Weller M, Fisher B, Taphoorn MJ *et al*. Radiotherapy plus concomitant and adjuvant temozolomide for glioblastoma. N Engl J Med 2005; 352: 987-996.

2 Wick W, Stupp R, Beule AC, Bromberg J, Wick A, Ernemann U *et al*. A novel tool to analyze MRI recurrence patterns in glioblastoma. Neuro Oncol 2008; 10: 1019-1024.

3 Moon RT, Brown JD, Torres M. WNTs modulate cell fate and behavior during vertebrate development. Trends Genet 1997; 13: 157-162.

4 van de Wetering M, Sancho E, Verweij C, de Lau W, Oving I, Hurlstone A *et al*. The beta-catenin/TCF-4 complex imposes a crypt progenitor phenotype on colorectal cancer cells. Cell 2002; 111: 241-250.

5 Reya T, Clevers H. Wnt signalling in stem cells and cancer. Nature 2005; 434: 843-850.

6 Boerboom D, White LD, Dalle S, Courty J, Richards JS. Dominant-stable beta-catenin expression causes cell fate alterations and Wnt signalling antagonist expression in a murine granulosa cell tumor model. Cancer Res 2006; 66: 1964-1973.

7 Voloshanenko O, Erdmann G, Dubash TD, Augustin I, Metzig M, Moffa G *et al*. Wnt secretion is required to maintain high levels of Wnt activity in colon cancer cells. Nat Commun 2013; 4: 2610.

8 Polakis P. Wnt signalling in cancer. Cold Spring Harb Perspect Biol 2012; 4.

9 Cheng R, Sun B, Liu Z, Zhao X, Qi L, Li Y *et al*. Wnt5a Suppresses Colon Cancer by Inhibiting Cell Proliferation and Epithelial-Mesenchymal Transition. J Cell Physiol 2014.

10 Lambiv WL, Vassallo I, Delorenzi M, Shay T, Diserens AC, Misra A *et al*. The Wnt inhibitory factor 1 (WIF1) is targeted in glioblastoma and has a tumor suppressing function potentially by induction of senescence. Neuro Oncol 2011; 13: 736-747.

11 Gotze S, Wolter M, Reifenberger G, Muller O, Sievers S. Frequent promoter hypermethylation of Wnt pathway inhibitor genes in malignant astrocytic gliomas. Int J Cancer 2010; 126: 2584-2593.

12 Morris LG, Kaufman AM, Gong Y, Ramaswami D, Walsh LA, Turcan S *et al*. Recurrent somatic mutation of FAT1 in multiple human cancers leads to aberrant Wnt activation. Nat Genet 2013; 45: 253-261.

13 Gong A, Huang S. FoxM1 and Wnt/beta-catenin signalling in glioma stem cells. Cancer Res 2012; 72: 5658-5662.

14 Kamino M, Kishida M, Kibe T, Ikoma K, Iijima M, Hirano H *et al*. Wnt-5a signalling is correlated with infiltrative activity in human glioma by inducing cellular migration and MMP-2. Cancer Sci 2011; 102: 540-548.

15 Yu JM, Jun ES, Jung JS, Suh SY, Han JY, Kim JY *et al*. Role of Wnt5a in the proliferation of human glioblastoma cells. Cancer Lett 2007; 257: 172-181.

16 Kawano Y, Kypta R. Secreted antagonists of the Wnt signalling pathway. J Cell Sci 2003; 116: 2627-2634.

17 Enomoto M, Hayakawa S, Itsukushima S, Ren DY, Matsuo M, Tamada K *et al*. Autonomous regulation of osteosarcoma cell invasiveness by Wnt5a/Ror2 signalling. Oncogene 2009; 28: 3197-3208.

18 Nishita M, Yoo SK, Nomachi A, Kani S, Sougawa N, Ohta Y *et al*. Filopodia formation mediated by receptor tyrosine kinase Ror2 is required for Wnt5a-induced cell migration. J Cell Biol 2006; 175: 555-562.

19 Oishi I, Suzuki H, Onishi N, Takada R, Kani S, Ohkawara B *et al*. The receptor tyrosine kinase Ror2 is involved in non-canonical Wnt5a/JNK signalling pathway. Genes Cells 2003; 8: 645-654.

20 Semenov MV, Habas R, Macdonald BT, He X. SnapShot: Noncanonical Wnt Signalling Pathways. Cell 2007; 131: 1378.

21 De A. Wnt/Ca2+ signalling pathway: a brief overview. Acta Biochim Biophys Sin (Shanghai) 2011; 43: 745-756.

22 Ma L, Wang HY. Mitogen-activated protein kinase p38 regulates the Wnt/cyclic GMP/Ca2+ non-canonical pathway. J Biol Chem 2007; 282: 28980-28990.

23 Murat A, Migliavacca E, Gorlia T, Lambiv WL, Shay T, Hamou MF *et al*. Stem cell-related "self-renewal" signature and high epidermal growth factor receptor expression associated with resistance to concomitant chemoradiotherapy in glioblastoma. J Clin Oncol 2008; 26: 3015-3024.

24 Brennan CW, Verhaak RG, McKenna A, Campos B, Noushmehr H, Salama SR *et al*. The somatic genomic landscape of glioblastoma. Cell 2013; 155: 462-477.

25 Li G, Zhang H, Wan X, Yang X, Zhu C, Wang A *et al*. Long noncoding RNA plays a key role in metastasis and prognosis of hepatocellular carcinoma. Biomed Res Int 2014; 2014: 780521.

26 Tano K, Mizuno R, Okada T, Rakwal R, Shibato J, Masuo Y *et al*. MALAT-1 enhances cell motility of lung adenocarcinoma cells by influencing the expression of motility-related genes. FEBS Lett 2010; 584: 4575-4580.

27 Tripathi V, Ellis JD, Shen Z, Song DY, Pan Q, Watt AT *et al*. The nuclear-retained noncoding RNA MALAT1 regulates alternative splicing by modulating SR splicing factor phosphorylation. Mol Cell 2010; 39: 925-938.

28 Xu C, Yang M, Tian J, Wang X, Li Z. MALAT-1: a long non-coding RNA and its important 3' end functional motif in colorectal cancer metastasis. Int J Oncol 2011; 39: 169-175.

29 Yamamoto H, Oue N, Sato A, Hasegawa Y, Matsubara A, Yasui W *et al*. Wnt5a signalling is involved in the aggressiveness of prostate cancer and expression of metalloproteinase. Oncogene 2010; 29: 2036-2046.

30 Bitler BG, Nicodemus JP, Li H, Cai Q, Wu H, Hua X *et al*. Wnt5a suppresses epithelial ovarian cancer by promoting cellular senescence. Cancer Res 2011; 71: 6184-6194.

31 Liang H, Chen Q, Coles AH, Anderson SJ, Pihan G, Bradley A *et al*. Wnt5a inhibits B cell proliferation and functions as a tumor suppressor in hematopoietic tissue. Cancer Cell 2003; 4: 349-360.

32 Ying J, Li H, Yu J, Ng KM, Poon FF, Wong SC *et al*. WNT5A exhibits tumor-suppressive activity through antagonizing the Wnt/beta-catenin signalling, and is frequently methylated in colorectal cancer. Clin Cancer Res 2008; 14: 55-61.

33 Kremenevskaja N, von Wasielewski R, Rao AS, Schofl C, Andersson T, Brabant G. Wnt-5a has tumor suppressor activity in thyroid carcinoma. Oncogene 2005; 24: 2144-2154.

34 Habu M, Koyama H, Kishida M, Kamino M, Iijima M, Fuchigami T *et al*. Ryk is essential for Wnt-5a-dependent invasiveness in human glioma. J Biochem 2014.

35 Pulvirenti T, Van Der Heijden M, Droms LA, Huse JT, Tabar V, Hall A. Dishevelled 2 signalling promotes self-renewal and tumorigenicity in human gliomas. Cancer Res 2011; 71: 7280-7290.

36 Ono K, Han J. The p38 signal transduction pathway: activation and function. Cell Signal 2000; 12: 1-13.

37 Zhang Z, Lv J, Lei X, Li S, Zhang Y, Meng L *et al*. Baicalein reduces the invasion of glioma cells via reducing the activity of p38 signalling pathway. PLoS One 2014; 9: e90318.

38 Demuth T, Reavie LB, Rennert JL, Nakada M, Nakada S, Hoelzinger DB *et al*. MAP-ing glioma invasion: mitogen-activated protein kinase kinase 3 and p38 drive glioma invasion and progression and predict patient survival. Mol Cancer Ther 2007; 6: 1212-1222.

39 Greenberg AK, Basu S, Hu J, Yie TA, Tchou-Wong KM, Rom WN *et al*. Selective p38 activation in human non-small cell lung cancer. Am J Respir Cell Mol Biol 2002; 26: 558-564.

40 Besson A, Davy A, Robbins SM, Yong VW. Differential activation of ERKs to focal adhesions by PKC epsilon is required for PMA-induced adhesion and migration of human glioma cells. Oncogene 2001; 20: 7398-7407.

41 Chuderland D, Seger R. Calcium regulates ERK signalling by modulating its protein-protein interactions. Commun Integr Biol 2008; 1: 4-5.

42 Hutchinson JN, Ensminger AW, Clemson CM, Lynch CR, Lawrence JB, Chess A. A screen for nuclear transcripts identifies two linked noncoding RNAs associated with SC35 splicing domains. BMC Genomics 2007; 8: 39.

43 Wang Y, Jiang T. Understanding high grade glioma: molecular mechanism, therapy and comprehensive management. Cancer Lett 2012; 331: 139-146.

44 Ishii N, Maier D, Merlo A, Tada M, Sawamura Y, Diserens AC *et al*. Frequent co-alterations of TP53, p16/CDKN2A, p14ARF, PTEN tumor suppressor genes in human glioma cell lines. Brain Pathol 1999; 9: 469-479.

45 Sciuscio D, Diserens AC, van Dommelen K, Martinet D, Jones G, Janzer RC *et al*. Extent and patterns of MGMT promoter methylation in glioblastoma- and respective glioblastoma-derived spheres. Clin Cancer Res 2011; 17: 255-266.

46 Bady P, Diserens AC, Castella V, Kalt S, Heinimann K, Hamou MF *et al*. DNA fingerprinting of glioma cell lines and considerations on similarity measurements. Neuro Oncol 2012; 14: 701-711.

47 Comprehensive genomic characterization defines human glioblastoma genes and core pathways. Nature 2008; 455: 1061-1068.

48 Petrova TV, Nykanen A, Norrmen C, Ivanov KI, Andersson LC, Haglund C *et al*. Transcription factor PROX1 induces colon cancer progression by promoting the transition from benign to highly dysplastic phenotype. Cancer Cell 2008; 13: 407-419.

49 Gossen M, Freundlieb S, Bender G, Muller G, Hillen W, Bujard H. Transcriptional activation by tetracyclines in mammalian cells. Science 1995; 268: 1766-1769.

50 Morgenstern JP, Land H. A series of mammalian expression vectors and characterisation of their expression of a reporter gene in stably and transiently transfected cells. Nucleic Acids Res 1990; 18: 1068.

51 Schneider CA, Rasband WS, Eliceiri KW. NIH Image to ImageJ: 25 years of image analysis. Nat Methods 2012; 9: 671-675.

52 Cawthorne C, Swindell R, Stratford IJ, Dive C, Welman A. Comparison of doxycycline delivery methods for Tet-inducible gene expression in a subcutaneous xenograft model. J Biomol Tech 2007; 18: 120-123.

53 Andreeff M, Ruvolo V, Gadgil S, Zeng C, Coombes K, Chen W *et al*. HOX expression patterns identify a common signature for favorable AML. Leukemia 2008; 22: 2041-2047.

54 Lal M, Song X, Pluznick JL, Di Giovanni V, Merrick DM, Rosenblum ND *et al*. Polycystin-1 C-terminal tail associates with beta-catenin and inhibits canonical Wnt signalling. Hum Mol Genet 2008; 17: 3105-3117.

55 O'Connell MP, Fiori JL, Baugher KM, Indig FE, French AD, Camilli TC *et al*. Wnt5A activates the calpain-mediated cleavage of filamin A. J Invest Dermatol 2009; 129: 1782-1789.

56 Li X, Zhou Q, Hanus J, Anderson C, Zhang H, Dellinger M *et al*. Inhibition of multiple pathogenic pathways by histone deacetylase inhibitor SAHA in a corneal alkali-burn injury model. Mol Pharm 2013; 10: 307-318.

57 Untergasser A, Cutcutache I, Koressaar T, Ye J, Faircloth BC, Remm M *et al*. Primer3--new capabilities and interfaces. Nucleic Acids Res 2012; 40: e115.

58 Gentleman RC, Carey VJ, Bates DM, Bolstad B, Dettling M, Dudoit S *et al*. Bioconductor: open software development for computational biology and bioinformatics. Genome Biol 2004; 5: R80.

59 Gautier L, Cope L, Bolstad BM, Irizarry RA. affy--analysis of Affymetrix GeneChip data at the probe level. Bioinformatics 2004; 20: 307-315.

Figure Legends:

Figure 1. Regulation of the canonical and non-canonical WNT-pathways by WIF1.

(A) TOP flash/FOP flash reporter system was used to test the transactivation of β-catenin, and the AP1 reporter to test the JNK/WNT pathway. LN-229_ind*WIF1* cells were transfected with the reporter plasmids 72h prior luciferase measurements and DOX was added 48h before pathway analysis. LEF1-β-catenin fusion protein expression was used as positive control for the canonical WNT pathway, while for the AP1 reporter system cells were treated with phorbol-12-myristate-13-acetate (PMA) for 6h (200 nM). Results are normalized to the control. (B) The intracellular [Ca^{2+}] was measured using the FluoForte fluorescence kit, 48h after transfectionwith either the *WIF1* expression vector or the respective empty vector.

Figure 2. *WIF1* expression inhibits p38_MAPK phosphorylation.

(A) Images of the phospho-kinase protein arrays probed with protein extracts of LN-229_ind*WIF1* +/- DOX are shown. Differentially expressed proteins are highlighted with color boxes, and respective quantification is shown in (B). (C) Western blot analysis of LN-229 cells transiently transduced with either pcDNA3.1or pcDNA3.1_*WIF1,* 72h post-transfection. Densitometric quantification of the ratio between the *WIF1* expressing cells and the controls of three biological replicates are shown in (D). All proteins are normalized to α-Tubulin. (E) Intracellular [Ca^{2+}] was measured 48h after treatment with the p38-MAPK inhibitors SB203580 [10μM] and SB239063 [20μM].

Figure 3. *WNT5A* depletion recapitulates *WIF1*-induced alterations.

(A) The heat map shows the log fold change in expression of WNT ligands between GBM and non-tumoral brain in our own GBM dataset (GBM=70, non tumoral brain=4) [23] and the one from TCGA (GBM=573, Non Tumoral Brain=10) (B) Western blot of phosho-proteins 72h after knock down of *WNT5A* in LN-229 transfecting two specific siRNAs and respective scrambled controls. Densitometric quantification of the ratios between the si*WNT5A* expressing cells and the scrambled control are shown for three biological replicates (C). All quantifications are normalised to α-Tubulin.(D) The intracellular [Ca^{2+}] were measured 72h after transfection with either siScrambled or two specific *WNT5A* siRNAs.

Figure 4. *WIF1* expression inhibits migration

LN-229_ind*WIF1* were induced 48h with DOX (1 µg/mL), seeded on the upper membrane of the transwell and after 16h the cells that had migrated to the lower side of the membrane were quantified by crystal violet staining (A). In the wound-healing assay cells were induced with DOX for 24h, the scratch was made and allowed to heal for 24 and 48h, respectively, and the uncovered area was quantified (B).

A growth curve was performed over 6 days (C) to exclude *WIF1* mediated reduction in growth as potential confounding factor. DOX was added at T zero (24h after seeding).

Figure 5. *WIF1* expression inhibits migration *in vivo*.

(A) The GS-line LN-2669GS_*WIF1* stably expressing *WIF1* was compared to the

respective empty vector control LN-2669GS_pIRES2 using the limiting dilution sphere formation assay. The effect was quantified using a linear regression between negative wells (no sphere detected) and the no. of cells per well. (B) In vivo tumorigenicity was tested using an orthotopic xenograft model, mice were injected with either LN-2669GS_pIRES2 or LN-2669GS_*WIF1*. Mice were euthanized at first signs of neurological symptoms or weight loss. WIF1-mediated impact on migration was assessed by comparing the ratio of the number of human tumor cells, identified by the human specific antibody anti Nucleolin, on the contra-lateral side over the number of tumor cells on the injected side (model shown in (C), see methods for details) (D). Representative images of the histological analysis of tumour bearing brains (E). Scale bar = 50µm.

Figure 6. *WIF1* affects the expression of a key positive regulator of migration, *MALAT1*.

(A) The kinetics of *WIF1* induction was measured in LN229_ind*WIF1* by qRT-PCR and WIF1 secretion by ELISA. DOX was added at T zero (1 µg/ml). (B) Heat map of the top overexpressed and downregulated genes emerging from *WIF1*-induced differential gene expression profiles with at least a 2 fold change (log FC > |1|). (C) Confirmation of microarray data by qRT-PCR for *MALAT1*, WIF1-induction inhibits *MALAT1* expression and *AXIN2*. (D) *MALAT1* and *AXIN2* expression upon knock down of *WNT5A* in LN-229, as measured by qRT-PCR. (E) Treatment of LN-229 with the p38-MAPK inhibitor SB_203580 [10 µM] or SB239063 [20µM] reduced *MALAT1* expression as determined by qRT-PCR after 48h.

Figure 7. Downregulation of *MALAT1* inhibits migration of LN-229 cells.

(A) The expression of MALAT1 and of two known *MALAT1*-target genes was measured by qRT-PCR, upon knock-down of *MALAT1* using two disitinct siRNAs. The migration capability was tested by wound-healing assay (B, E) and the transwell assay (C, F) after *MALAT1* depletion in LN-229. In the wound-healing assay, the scratch was performed two days after transfection, and % coverage was quantified 24h later. For the transwell assay, two days after transfection the cells were seeded on the upper membrane, after 16h cells that had migrated to the lower side of the membrane were quantified by crystal violet staining. The growth curve of the transfected cells is shown in (D), excluding the proliferation rate as confounding factor (T zero, 24h after transfection).

Figure 8. Pathways alteration downstream of *WIF1* expression

Model for mechanisms implicated in WIF1-induced tumor suppressive phenotype. WIF1 inhibits both the canonical WNT-pathway and WNT5A-dependent non-canonicalWNT/Ca^{2+}/signalling. WIF1 dependent downregulation of the non-canonical WNT pathway results in reduction of p38-MAPK phosphorylation and a decrease in the intracellular [Ca^{2+}] as well as decreased expression of *MALAT1*. *MALAT1* is a long non-coding RNA involved in migration and its downregulation in GBM attenuates migration.

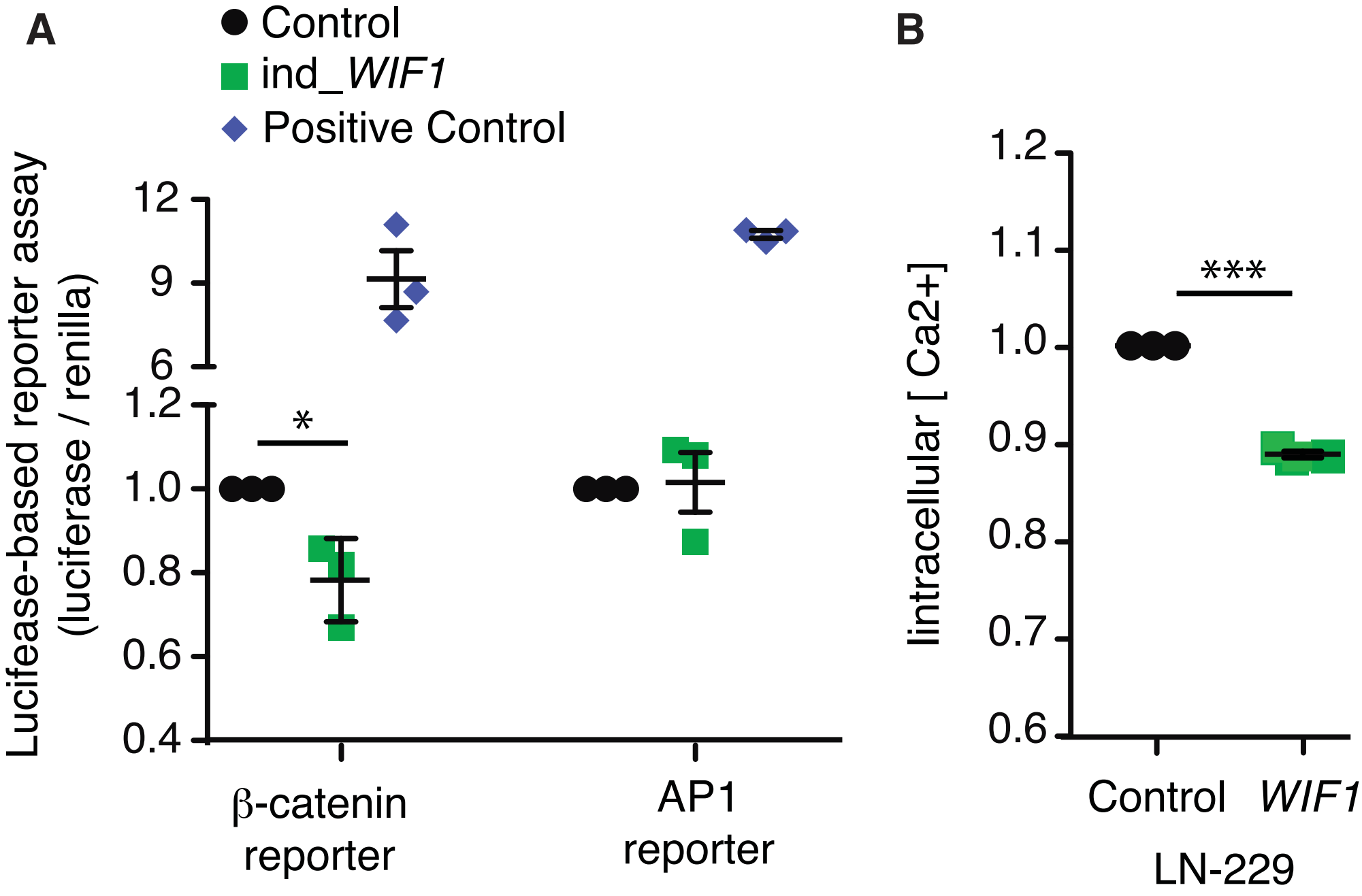
A
Control
ind_WIF1
Positive Control
Lucifease-based reporter assay
(luciferase / renilla)
12
9
6
1.2
1.0
0.8
0.6
0.4
*
β-catenin
reporter
AP1
reporter
B
Intracellular [Ca2+]
1.2
1.1
1.0
0.9
0.8
0.7
0.6
***
Control
WIF1
LN-229

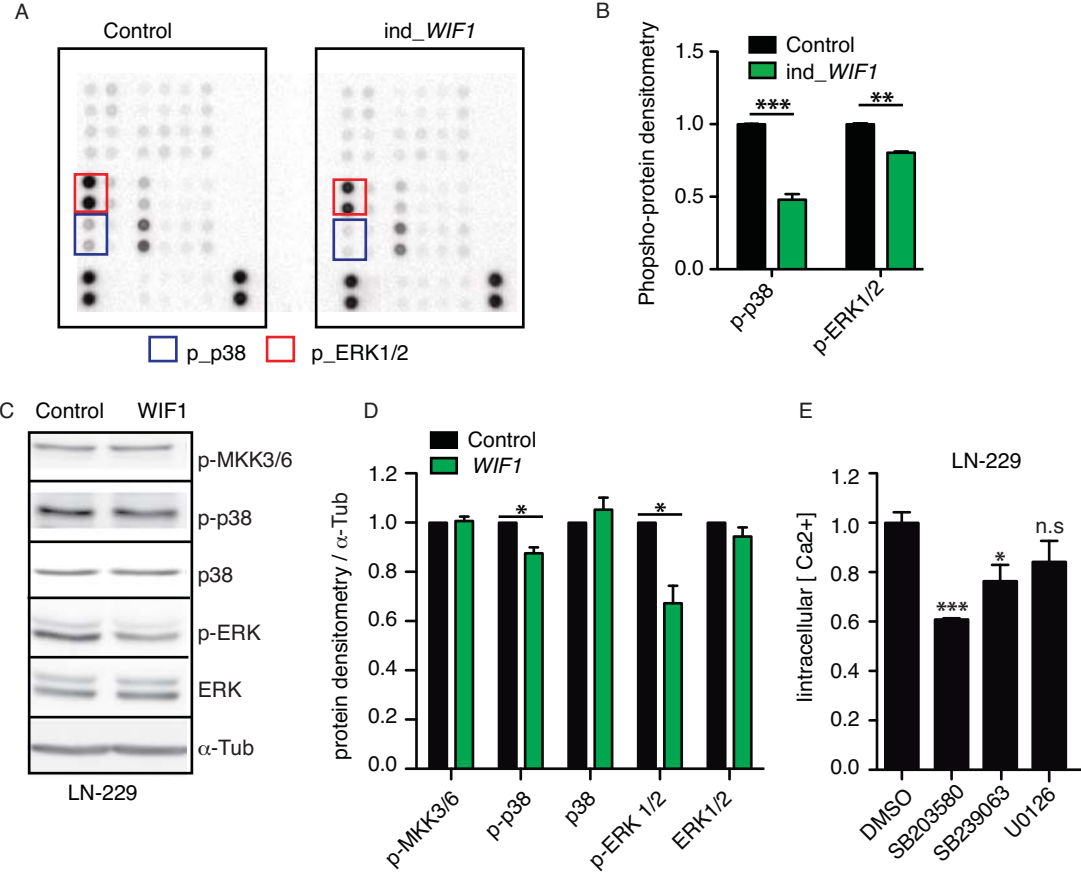
A
Control
ind_WIF1
p_p38
p_ERK1/2
B
Control
ind_WIF1
Phopsho-protein densitometry
1.5
1.0
0.5
0.0
***
**
p-p38
p-ERK1/2
C
Control
WIF1
p-MKK3/6
p-p38
p38
p-ERK
ERK
α-Tub
LN-229
D
Control
WIF1
protein densitometry / α-Tub
1.2
1.0
0.8
0.6
0.4
0.2
0.0
*
*
p-MKK3/6
p-p38
p38
p-ERK 1/2
ERK1/2
E
LN-229
lintracellular [Ca2+]
1.2
1.0
0.8
0.6
0.4
0.2
0.0
***
*
n.s
DMSO
SB203580
SB239063
U0126

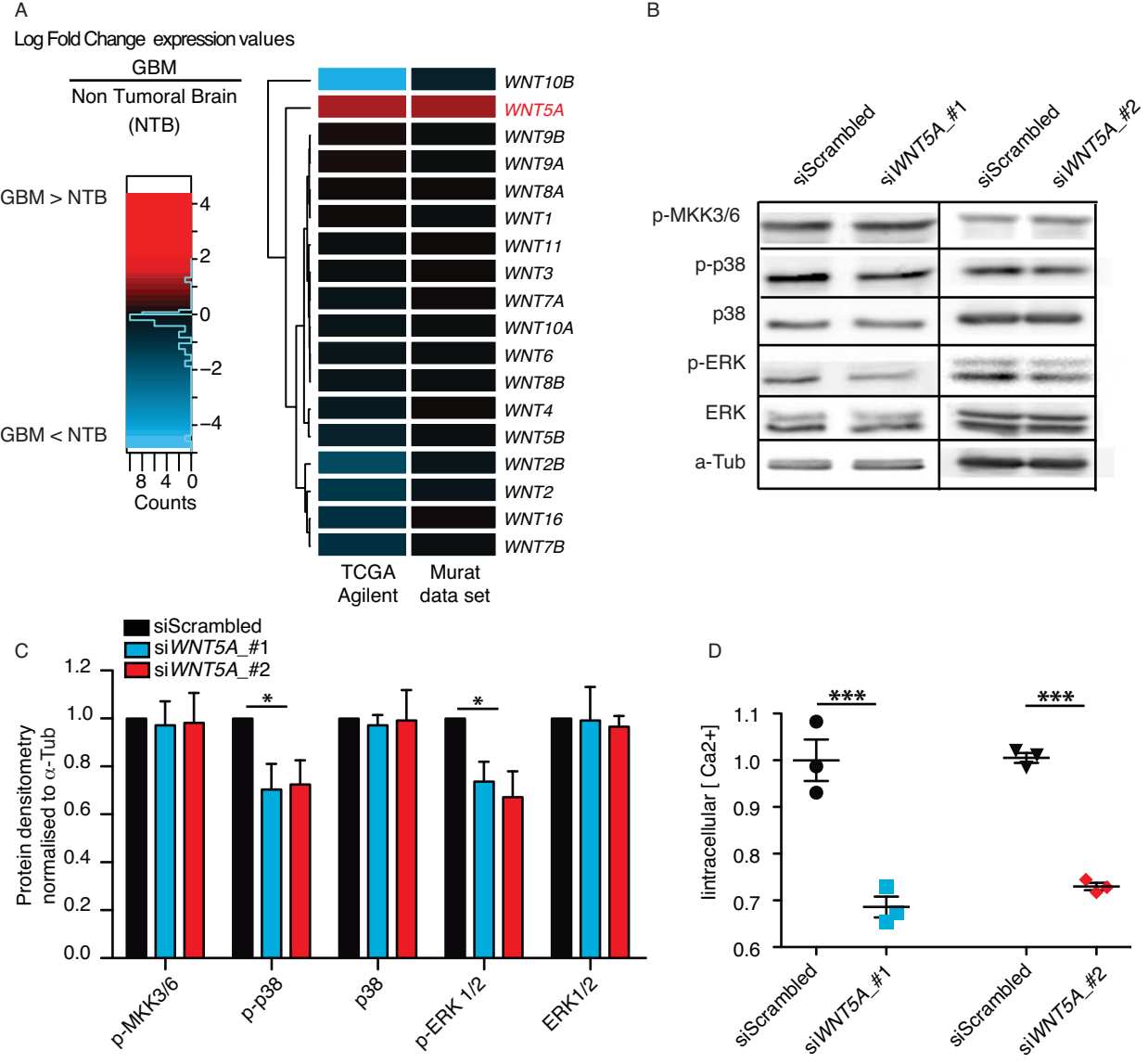
A
Log Fold Change expression values
GBM
Non Tumoral Brain
(NTB)
GBM > NTB
GBM < NTB
4
2
0
−2
−4
8 4 0
Counts
WNT10B
WNT5A
WNT9B
WNT9A
WNT8A
WNT1
WNT11
WNT3
WNT7A
WNT10A
WNT6
WNT8B
WNT4
WNT5B
WNT2B
WNT2
WNT16
WNT7B
TCGA Agilent
Murat data set
B
siScrambled
siWNT5A_#1
siScrambled
siWNT5A_#2
p-MKK3/6
p-p38
p38
p-ERK
ERK
a-Tub
C
siScrambled
siWNT5A_#1
siWNT5A_#2
Protein densitometry normalised to α-Tub
1.2
1.0
0.8
0.6
0.4
0.2
0.0
*
*
p-MKK3/6
p-p38
p38
p-ERK 1/2
ERK1/2
D
lintracellular [Ca2+]
1.1
1.0
0.9
0.8
0.7
0.6
***
***
siScrambled
siWNT5A_#1
siScrambled
siWNT5A_#2

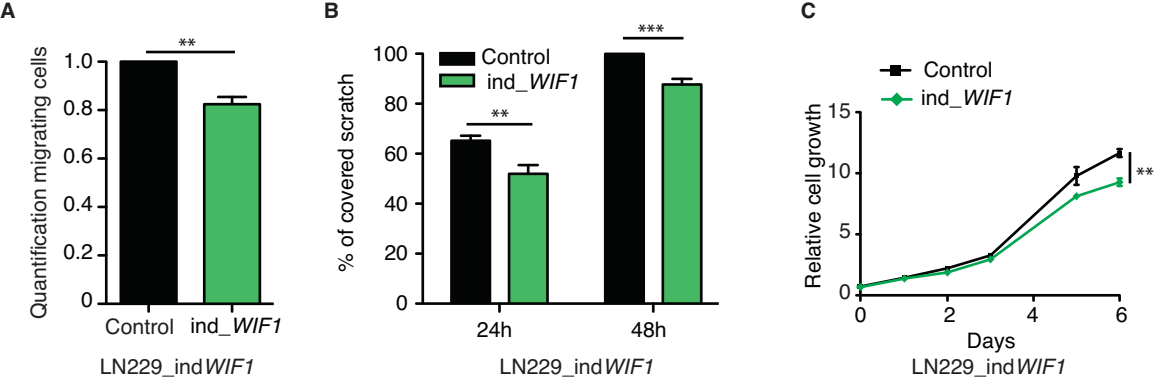
A
Quantification migrating cells
1.0
0.8
0.6
0.4
0.2
0
**
Control
ind_WIF1
LN229_ind WIF1
B
% of covered scratch
100
80
60
40
20
0
Control
ind_WIF1
**
***
24h
48h
LN229_ind WIF1
C
Relative cell growth
15
10
5
0
Control
ind_WIF1
**
0
2
4
6
Days
LN229_ind WIF1

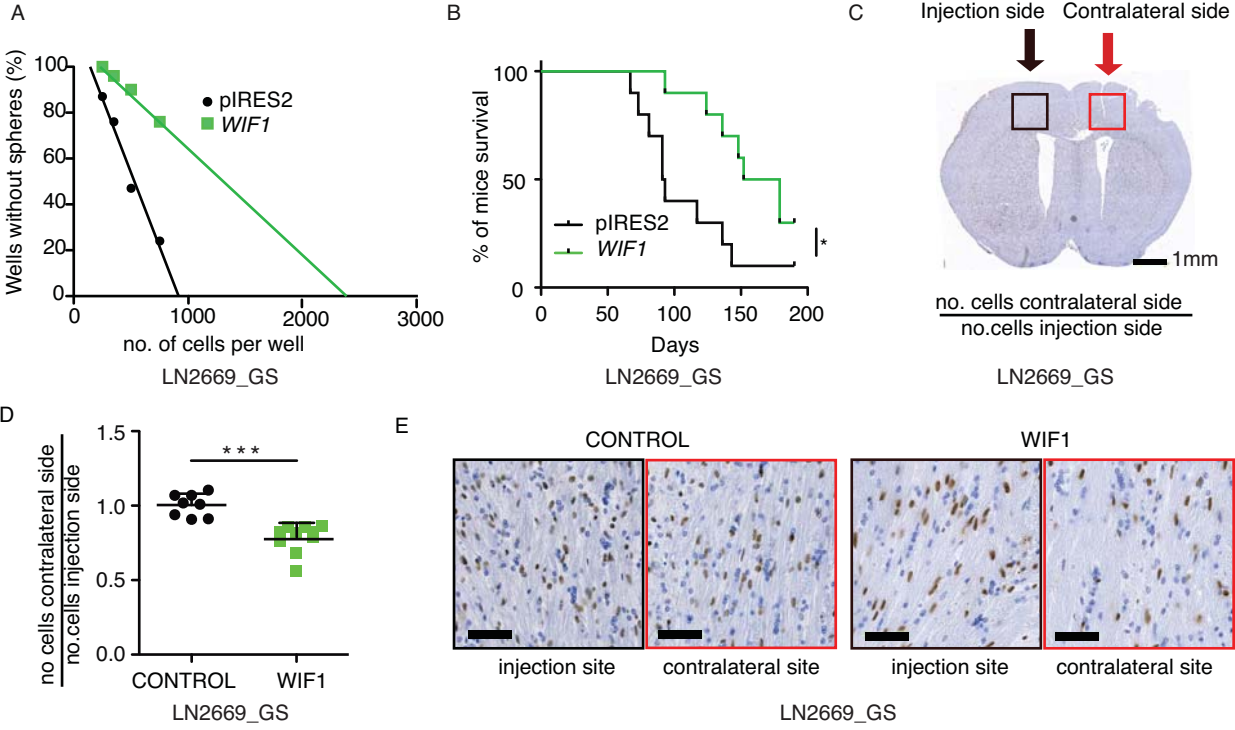
A
Wells without spheres (%)
100
80
60
40
20
0
pIRES2
WIF1
0
1000
2000
3000
no. of cells per well
LN2669_GS
B
% of mice survival
100
50
0
pIRES2
WIF1
*
0
50
100
150
200
Days
LN2669_GS
C
Injection side
Contralateral side
1mm
no. cells contralateral side
no.cells injection side
LN2669_GS
D
no cells contralateral side
no.cells injection side
1.5
1.0
0.5
0.0
***
CONTROL
WIF1
LN2669_GS
E
CONTROL
WIF1
injection site
contralateral site
injection site
contralateral site
LN2669_GS

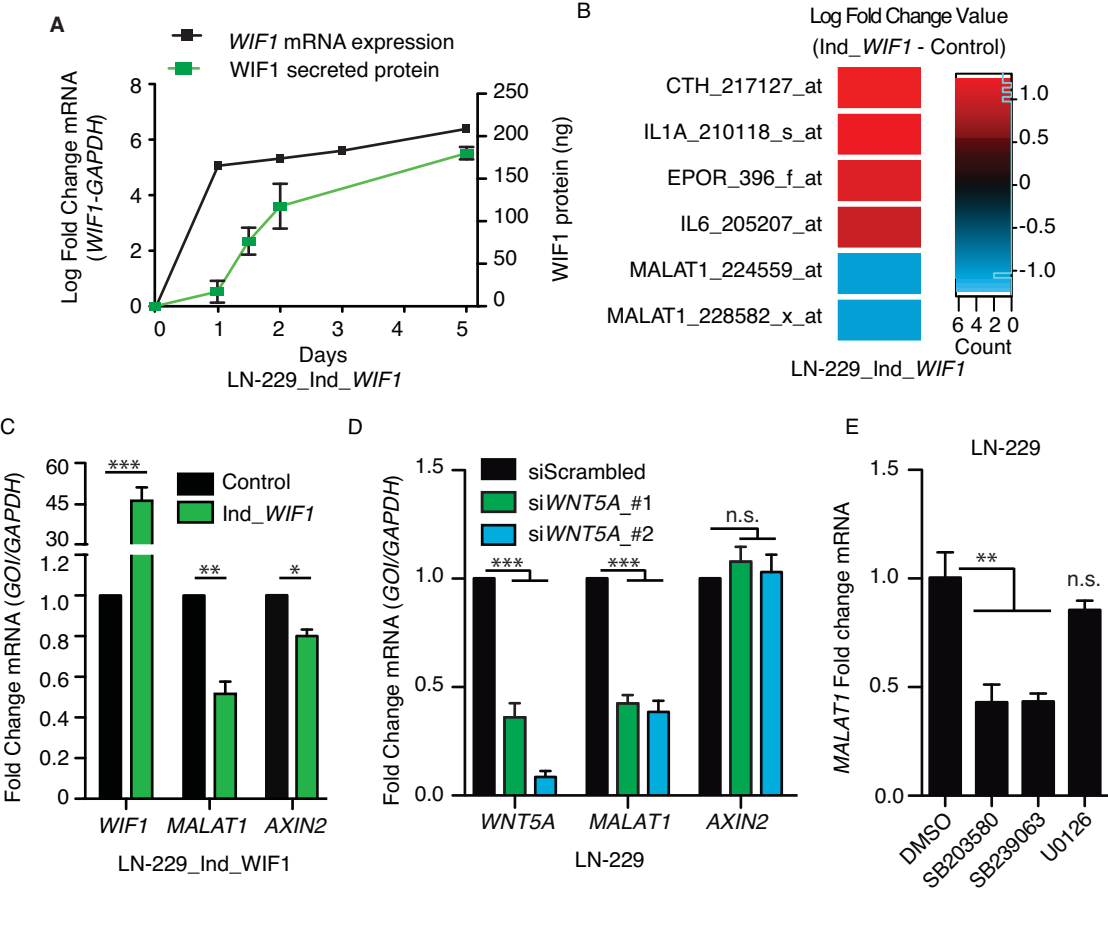
A
WIF1 mRNA expression
WIF1 secreted protein
Log Fold Change mRNA (WIF1-GAPDH)
WIF1 protein (ng)
Days
LN-229_Ind_WIF1
B
Log Fold Change Value
(Ind_WIF1 - Control)
CTH_217127_at
IL1A_210118_s_at
EPOR_396_f_at
IL6_205207_at
MALAT1_224559_at
MALAT1_228582_x_at
Count
LN-229_Ind_WIF1
C
Control
Ind_WIF1
Fold Change mRNA (GOI/GAPDH)
WIF1
MALAT1
AXIN2
LN-229_Ind_WIF1
D
siScrambled
siWNT5A_#1
siWNT5A_#2
n.s.
Fold Change mRNA (GOI/GAPDH)
WNT5A
MALAT1
AXIN2
LN-229
E
LN-229
MALAT1 Fold change mRNA
n.s.
DMSO
SB203580
SB239063
U0126

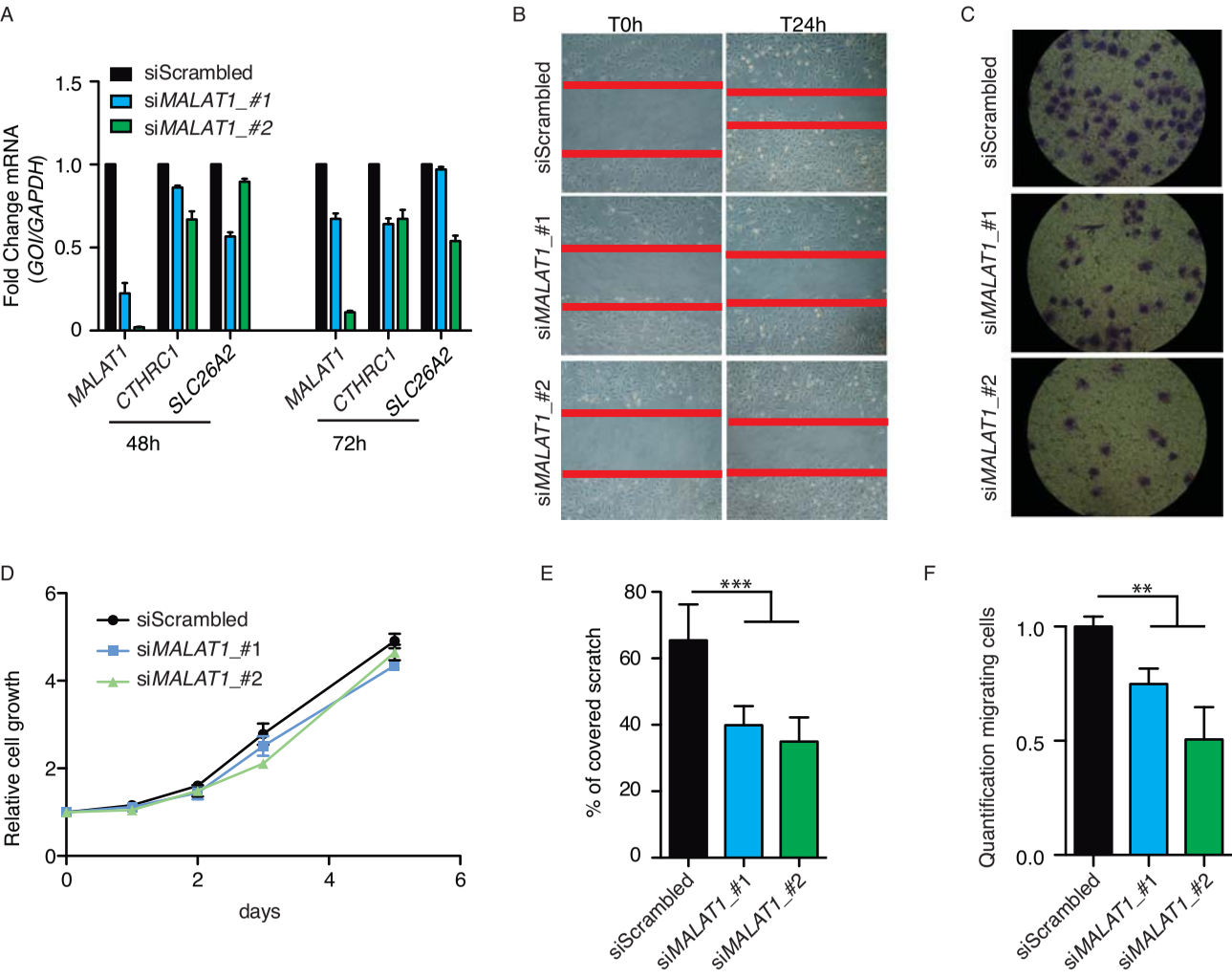
A
siScrambled
siMALAT1_#1
siMALAT1_#2
Fold Change mRNA (GOI/GAPDH)
1.5
1.0
0.5
0
MALAT1
CTHRC1
SLC26A2
MALAT1
CTHRC1
SLC26A2
48h
72h
B
T0h
T24h
siScrambled
siMALAT1_#1
siMALAT1_#2
C
siScrambled
siMALAT1_#1
siMALAT1_#2
D
siScrambled
siMALAT1_#1
siMALAT1_#2
Relative cell growth
6
4
2
0
0
2
4
6
days
E
% of covered scratch
80
60
40
20
0
***
siScrambled
siMALAT1_#1
siMALAT1_#2
F
Quantification migrating cells
1.0
0.5
0.0
**
siScrambled
siMALAT1_#1
siMALAT1_#2

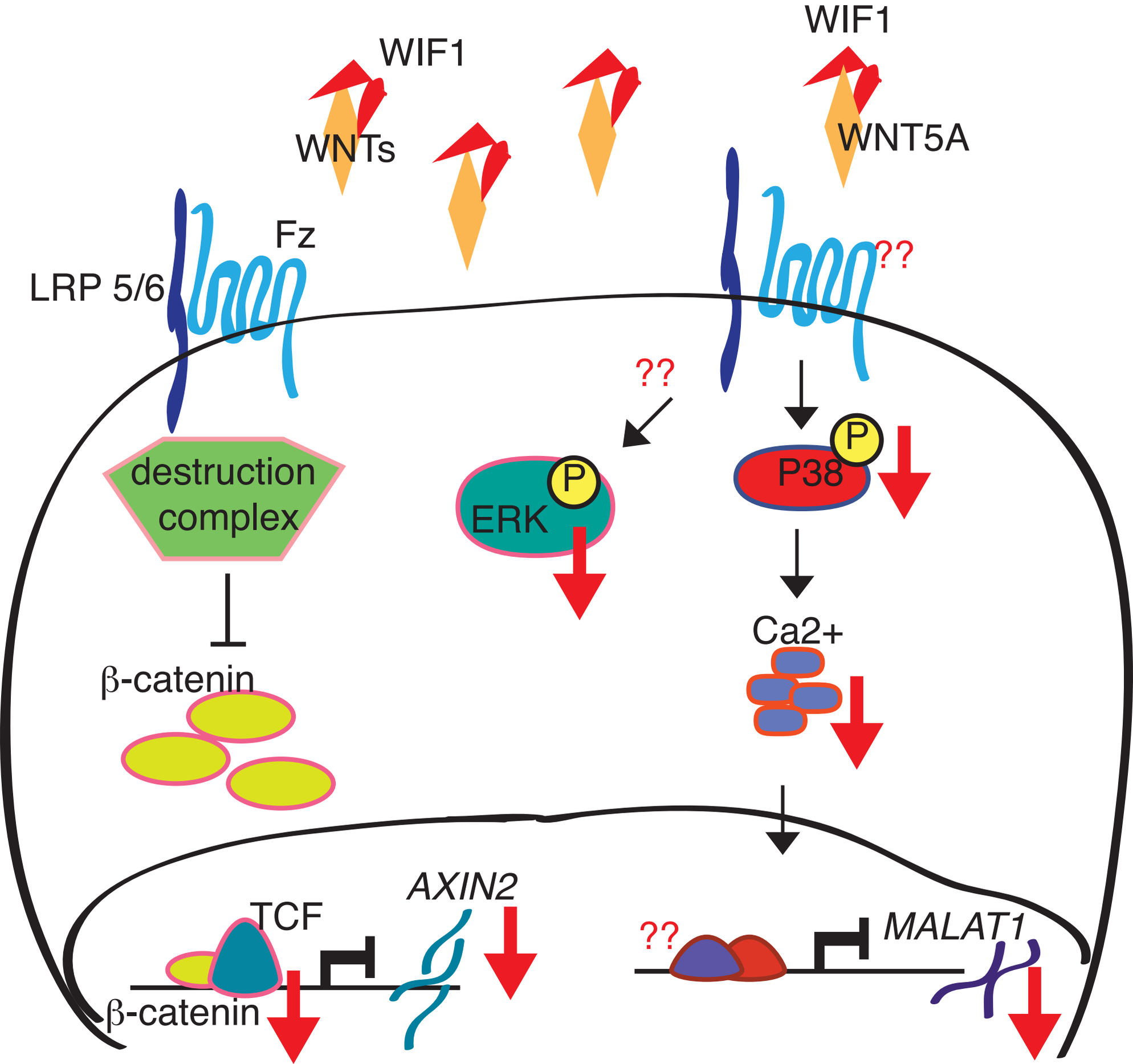
WIF1
WNTs
WIF1
WNT5A
Fz
LRP 5/6
??
??
destruction complex
ERK
P
P38
P
β-catenin
Ca2+
TCF
AXIN2
β-catenin
??
MALAT1

Supplemetary Information

Supplementary Figure Legends:

Figure S1. Analysis of the *in vivo* tumorigenicity of WIF1-induced glioma cell lines.

(A) Orthotopic injection of LN-229_ind*WIF1* (6 mice each group). WIF1 expression was induced feeding the mice with DOX-supplemented food. The supplemented food was changed every 2-3 days to avoid loss of DOX activity. The mice were euthanized at first signs of neurological symptoms or weight loss. (B) *WIF1* mRNA expression, measured by qRT-PCR, in the xenografts, suggests that expression was lost during the *in vivo* experiment.

Figure S2. Analysis of LN-229_ind_*dsRED* control cell line.

(A) DOX treatment induces *dsRED* expression. (B) Luciferase based-pathway analysis: TOP flash/FOP flash reporter system was used to test the transactivation of β-catenin and the AP1 reporter system to test the WNT/JNK pathway. LN-229_ind_*dsRED* cells were transfected with the reporter 72h prior luciferase measurements and DOX was added 48h before pathway analysis. Results are normalised to the control. (C) Cell proliferation was followed during 6 days upon *dsRED* induction. DOX was added at T zero (24h after seeding) (D) Migration analysis of LN229_ind_*dsRED* using the trans-well assay. LN229_ind_*dsRED* were induced with DOX (1 μg/mL) for 2 days. After the cells were trypsinized and seeded in the upper membrane of the trans-well. After 16h the cells that had migrated to the lower side of the membrane were quantified by crystal violet staining.

Figure S3. Western blot biological replicates

(A) Second and third biological replicates of Western blot analysis of LN-229 cells transiently transfected with either pcDNA3.1or pcDNA3.1_*WIF1,* 72h post-transfection, see Figure 2 (B) Second and third biological replicates of Western blot analysis 72h after knock down of *WNT5A* in LN-229, see Figure 3.

Figure S4. Inhibition of p38-MAPK and ERK

(A-B) phopho-MAPKAPK-2 and MAPKAPK-2 levels were measured by Western blot analysis in LN-229 treated with the p38-MAPK inhibitors, SB203580 and SB239063 at different concentrations (as reported in the graph). The red arrows indicate the concentrations used for the subsequent experiments. (C) Western blot quantification of phospho-ERK1/2, ERK1/2 in LN-229 treated with two p38-MAPK inhibitors: SB203580 and SB239063. (D) Western blot quantification of phospho-ERK1/2, ERK1/2, phopsho-p38-MAPK, p38-MAPK in LN-229 treated with the MEK1/2 inhibitor U0126.

Figure S5. Si*WNT5A* efficacy testing

(A) Three siRNAs with distinct sequences (Origene) were tested alone or in combination (Pooled_siRNA), and an additional siRNA from Ambion. The siRNAs were transfected at 25 nM final concentration. *WNT5A* mRNA was measured by qRT-PCR three days after transfection. *GAPDH* mRNA expression was used as housekeeping gene.

Figure S6. Confirmation of WIF1-dependent gene expression alteration

(A) qRT-PCR analysis of the genes found altered in the gene expression profile. The red arrows mark the transcripts that we confirmed as WIF1-dependent. (B-C) *MALAT1* expression was measured by qRT-PCR analysis in clones of the adherent cell line LN-319 (B) [10] and the glioma sphere line LN-2669-GS (C) stably expressing *WIF1*. *GAPDH* mRNA expression was used as housekeeping gene.

Figure S7. MALAT1 depletion inhibits migration in the cell lines: LN-18 and LN-428.

The effect of *MALAT1* depletion on migration was tested by wound-healing assay and the transwell assay in the GBM cell lines LN-18 (A-B) and LN-428 (D-E). In the wound-healing assay, the scratch was performed two days after transfection, and % coverage was quantified 24h later. For the transwell assay, two days after transfection the cells were seeded on the upper membrane, after 16h cells that had migrated to the lower side of the membrane were quantified by crystal violet staining. The growth curve of the transfected cells is shown in (C) and (F), respectively for LN-18 and LN-428, excluding the proliferation rate as confounding factor.

A

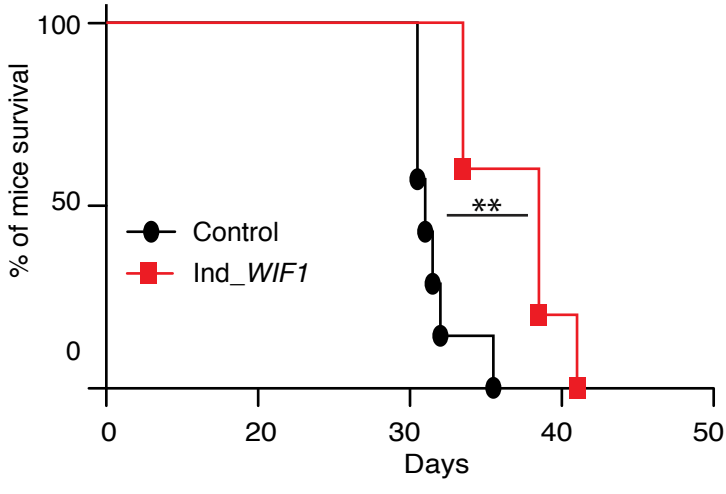
100
50
0
% of mice survival
Control
Ind_WIF1
**
0
20
30
40
50
Days

B

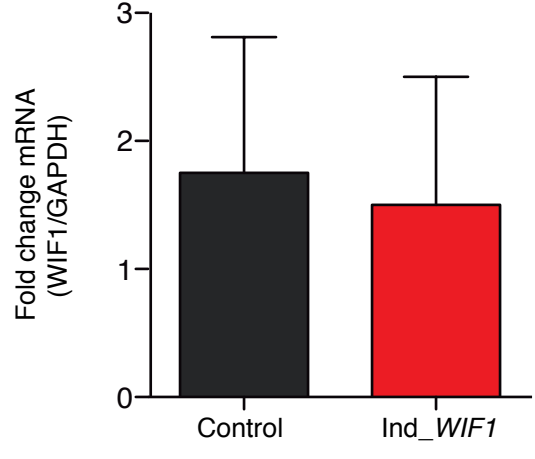
3
2
1
0
Fold change mRNA
(WIF1/GAPDH)
Control
Ind_WIF1

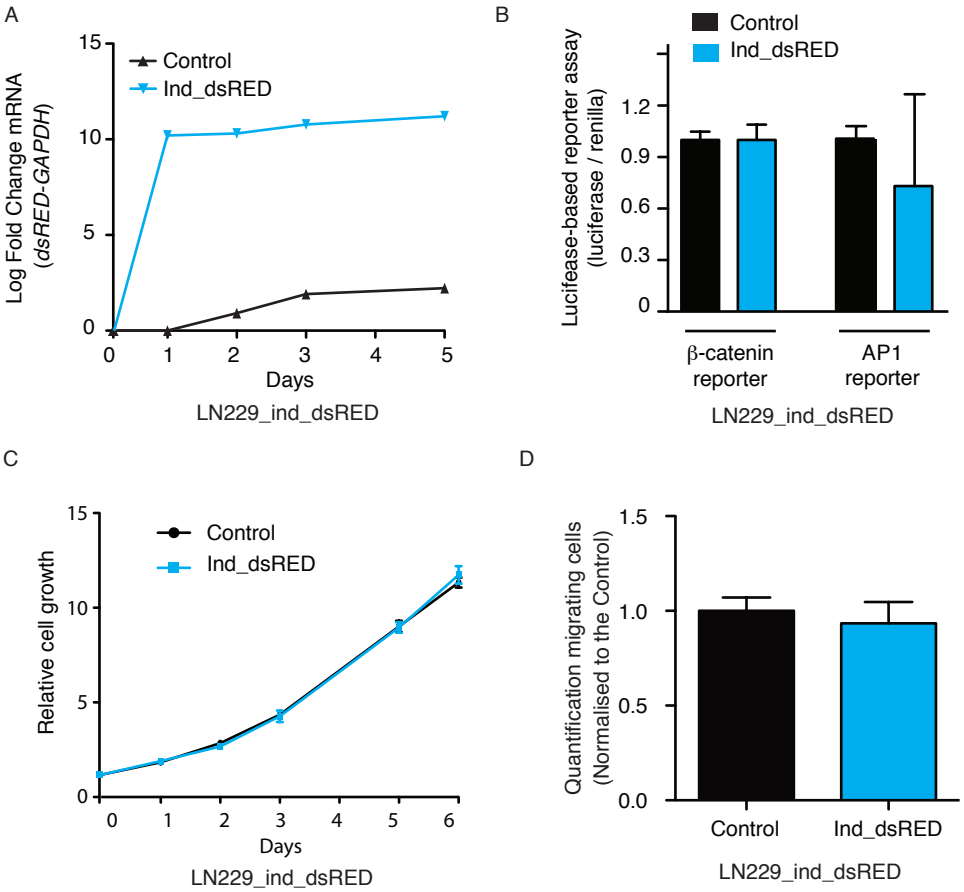
A
Log Fold Change mRNA
(dsRED-GAPDH)
15
10
5
0
Control
Ind_dsRED
0
1
2
3
4
5
Days
LN229_ind_dsRED
B
Control
Ind_dsRED
Lucifease-based reporter assay
(luciferase / renilla)
1.2
0.9
0.6
0.3
0
β-catenin
reporter
AP1
reporter
LN229_ind_dsRED
C
Relative cell growth
15
10
5
0
Control
Ind_dsRED
0
1
2
3
4
5
6
Days
LN229_ind_dsRED
D
Quantification migrating cells
(Normalised to the Control)
1.5
1.0
0.5
0.0
Control
Ind_dsRED
LN229_ind_dsRED

A)

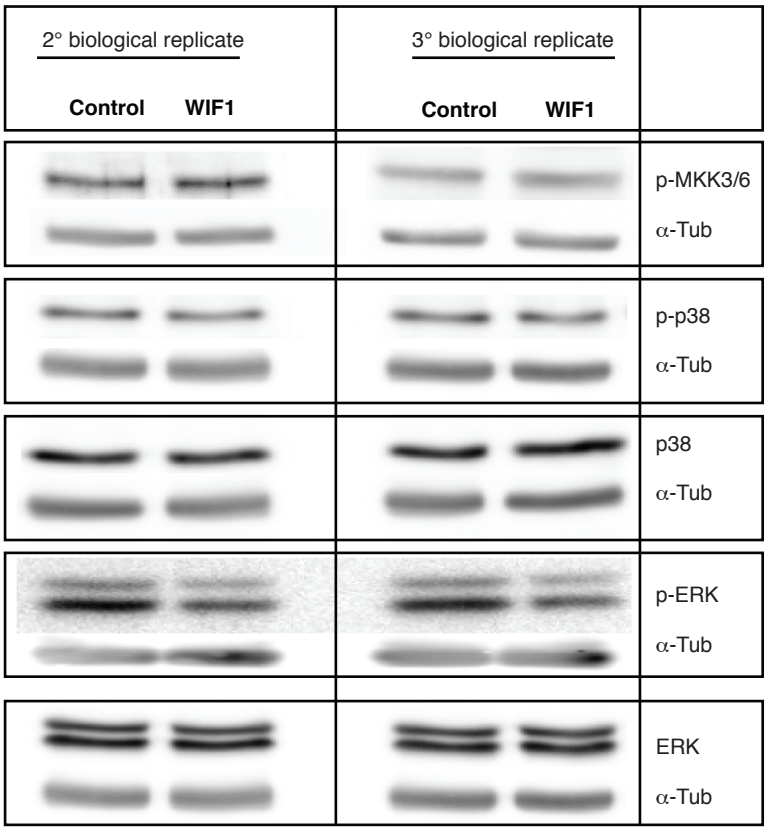
2° biological replicate
Control
WIF1
3° biological replicate
Control
WIF1
p-MKK3/6
α-Tub
p-p38
α-Tub
p38
α-Tub
p-ERK
α-Tub
ERK
α-Tub

B)

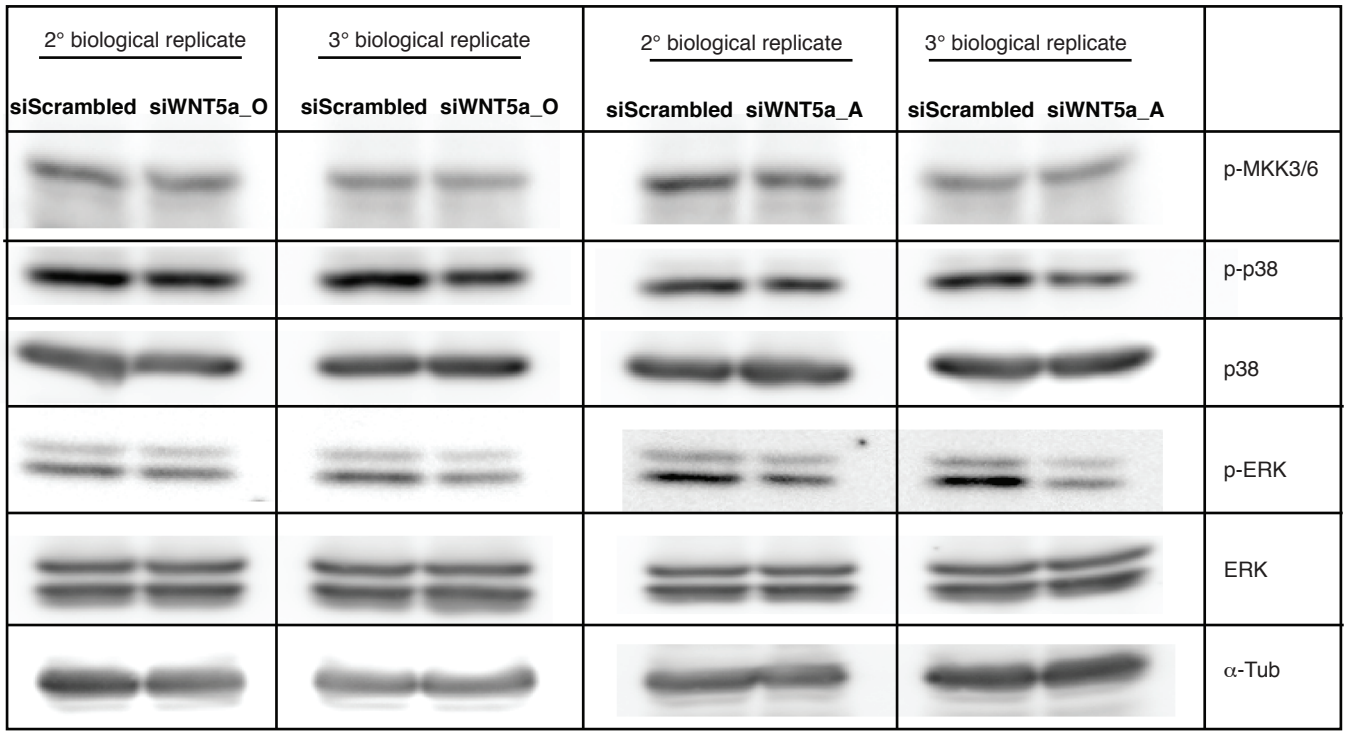
2° biological replicate
siScrambled
siWNT5a_O
3° biological replicate
siScrambled
siWNT5a_O
2° biological replicate
siScrambled
siWNT5a_A
3° biological replicate
siScrambled
siWNT5a_A
p-MKK3/6
p-p38
p38
p-ERK
ERK
α-Tub

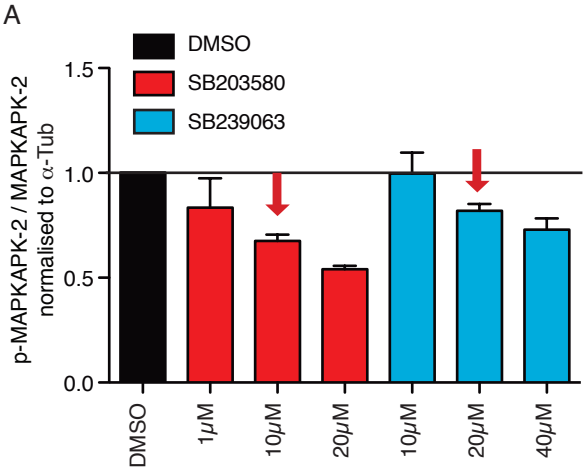
A
DMSO
SB203580
SB239063
p-MAPKAPK-2 / MAPKAPK-2
normalised to α-Tub
1.5
1.0
0.5
0.0
DMSO
1μM
10μM
20μM
10μM
20μM
40μM

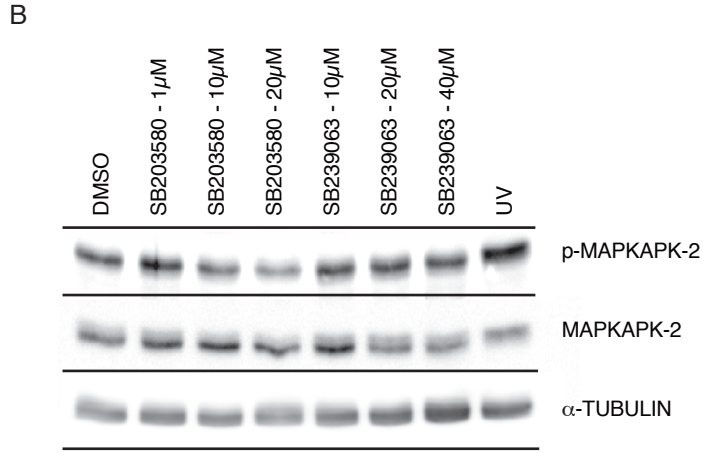
B
DMSO
SB203580 - 1μM
SB203580 - 10μM
SB203580 - 20μM
SB239063 - 10μM
SB239063 - 20μM
SB239063 - 40μM
UV
p-MAPKAPK-2
MAPKAPK-2
α-TUBULIN

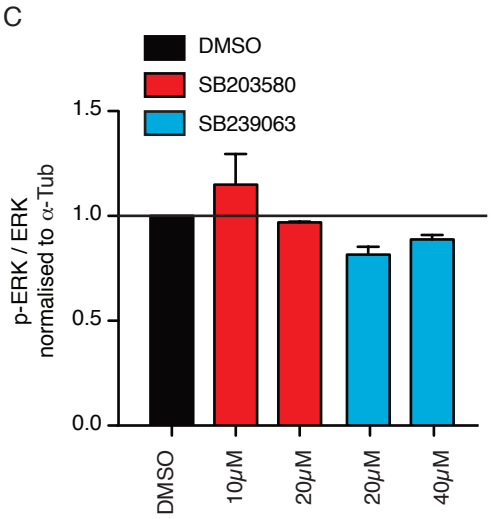
C
DMSO
SB203580
SB239063
p-ERK / ERK
normalised to α-Tub
1.5
1.0
0.5
0.0
DMSO
10μM
20μM
20μM
40μM

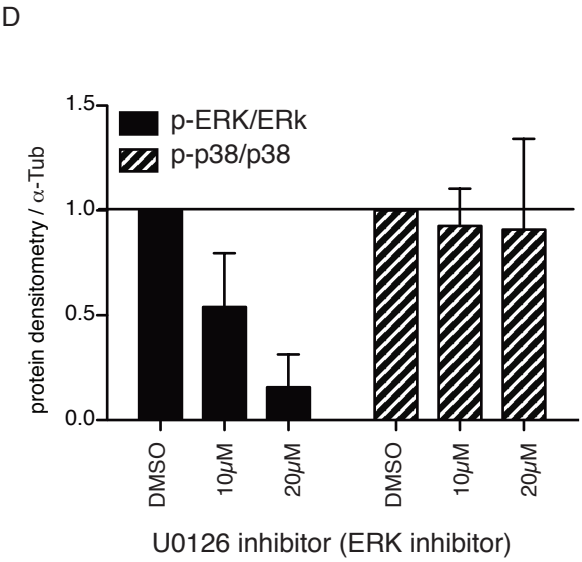
D
p-ERK/ERk
p-p38/p38
protein densitometry / α-Tub
1.5
1.0
0.5
0.0
DMSO
10μM
20μM
DMSO
10μM
20μM
U0126 inhibitor (ERK inhibitor)

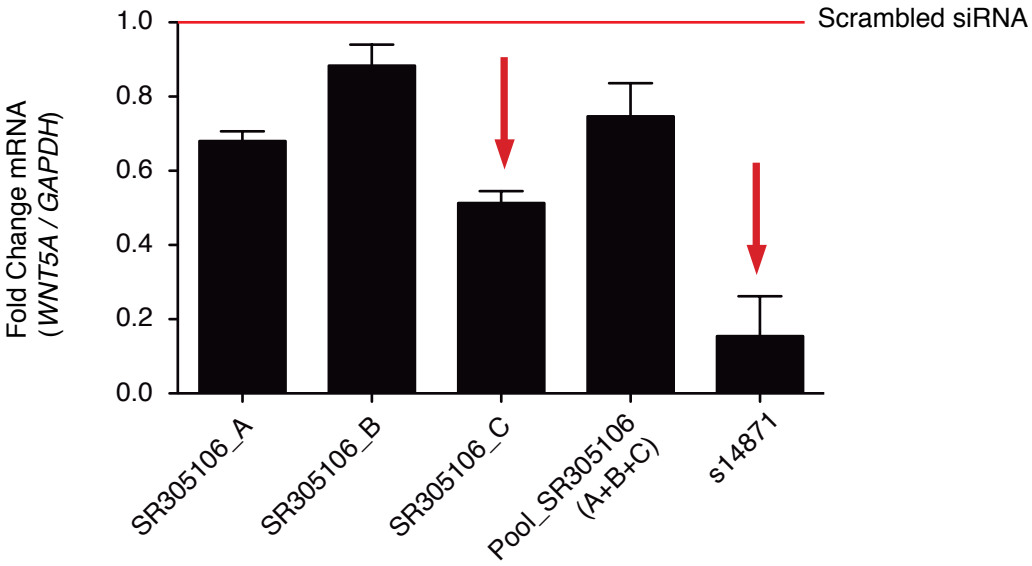
Scrambled siRNA
1.0
0.8
0.6
0.4
0.2
0.0
Fold Change mRNA
(WNT5A / GAPDH)
SR305106_A
SR305106_B
SR305106_C
Pool_SR305106
(A+B+C)
s14871

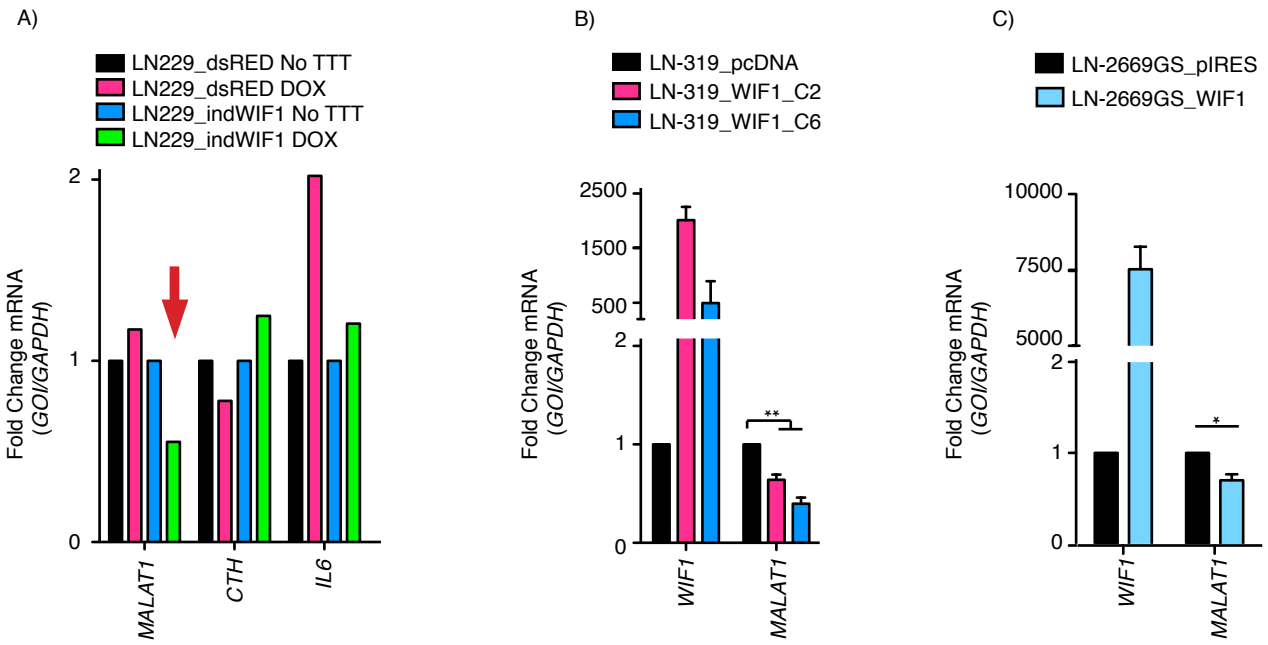
A)
LN229_dsRED No TTT
LN229_dsRED DOX
LN229_indWIF1 No TTT
LN229_indWIF1 DOX
Fold Change mRNA (GOI/GAPDH)
2
1
0
MALAT1
CTH
IL6
B)
LN-319_pcDNA
LN-319_WIF1_C2
LN-319_WIF1_C6
Fold Change mRNA (GOI/GAPDH)
2500
1500
500
2
1
0
**
WIF1
MALAT1
C)
LN-2669GS_pIRES
LN-2669GS_WIF1
Fold Change mRNA (GOI/GAPDH)
10000
7500
5000
2
1
0
*
WIF1
MALAT1

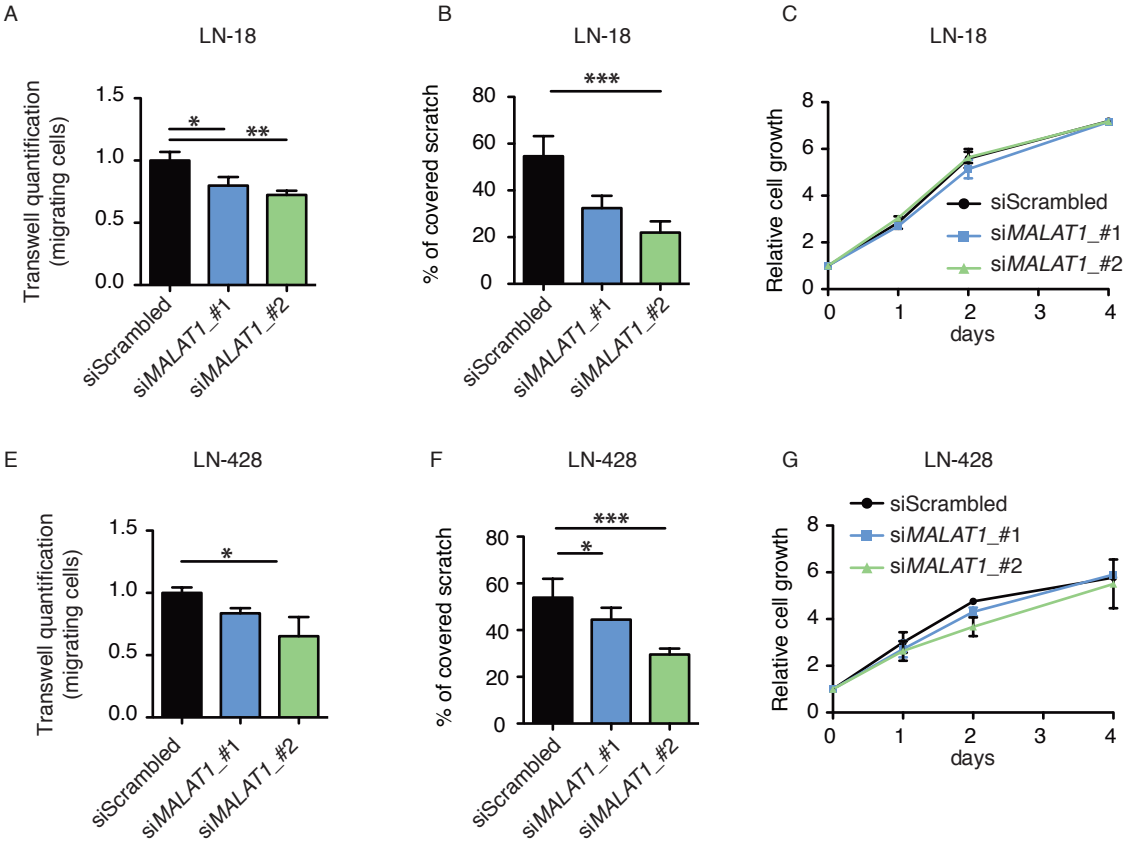
A
LN-18
Transwell quantification (migrating cells)
1.5
1.0
0.5
0.0
*
**
siScrambled
siMALAT1_#1
siMALAT1_#2
B
LN-18
% of covered scratch
80
60
40
20
0
***
siScrambled
siMALAT1_#1
siMALAT1_#2
C
LN-18
Relative cell growth
8
6
4
2
0
0
1
2
3
4
days
siScrambled
siMALAT1_#1
siMALAT1_#2
E
LN-428
Transwell quantification (migrating cells)
1.5
1.0
0.5
0.0
*
siScrambled
siMALAT1_#1
siMALAT1_#2
F
LN-428
% of covered scratch
80
60
40
20
0
***
*
siScrambled
siMALAT1_#1
siMALAT1_#2
G
LN-428
Relative cell growth
8
6
4
2
0
0
1
2
3
4
days
siScrambled
siMALAT1_#1
siMALAT1_#2

Supplementary Table 1: siRNAs information

Gene targeted	Purchased from:	Cat number:	Referred as:
Negative control	Origene	SR30004	
Negative control	Ambion	4390843	
WNT5A	Origene	SR305106A	
WNT5A	Origene	SR305106B	siWNT5A_#1
WNT5A	Origene	SR305106C	siWNT5A_#2
WNT5A	Ambion	4392420 (s14871)	
MALAT1	Ambion	4455877	siMALAT1_#1
MALAT1	Ambion	4390771 (n272231)	siMALAT1_#2

Supplementary Table 2. Primer sequence information

Gene	Forward (5’-3)	Reverse (5’-3)
CTH	CACTGTCCACCACGTTCAAG	TACTTAGCCCCATCCAGTGC
MALAT1	CTTCCCTAGGGGATTTCAGG	GATGCAAATGCCTCTGAGTG
CTHRC1	TGGACACCCAACTACAAGCA	GCATTTTAGCCGAAGTGAGC
SLC26A2	GTTTCAAATGGGAGCAC	GCCCATCGCTACCTGATAAA
IGFBP5	GGTTTGCCTCAACGAAAAGA	AGTAGGTCTCCTCGGCCATC
ALDH1L2	CCAGAGCCTCTTTGGACAAG	ACAGGGGTCCCATCTTTCTC